energies

MDPI

Article

Collaborative Optimization Framework for Coupled Power and Transportation Energy Systems Incorporating Integrated Demand Responses and Electric Vehicle Battery State-of-Charge

Lijun Geng [1,*], Chengxia Sun [1], Dongdong Song [1], Zilong Zhang [1], Chenyang Wang [1] and Zhigang Lu [2]

[1] Mechanical and Electrical Engineering College, Hebei Normal University of Science and Technology, Qinhuangdao 066004, China; sunchengxia2021@126.com (C.S.); 13903351740@126.com (D.S.); zhangzilong0630@163.com (Z.Z.); wangcy521@foxmail.com (C.W.)

[2] Key Lab of Power Electronics for Energy Conservation and Motor Drive of Hebei Province, Yanshan University, Qinhuangdao 066004, China; zhglu@ysu.edu.cn

* Correspondence: li_jungeng@163.com

Abstract: The growing adoption of electric vehicles (EVs) and advancements in dynamic wireless charging (DWC) technology have strengthened the interdependence between power distribution networks (PDNs) and electrified transportation networks (ETNs), leading to the emergence of coupled power and transportation energy systems (CPTESs). This development introduces new challenges, particularly as DWC technology shifts EV charging demand from residential plug-in charging to charging-while-driving during commuting hours, causing simultaneous congestion in both ETNs and PDNs during peak times. The present work addresses this issue by developing a collaborative optimization framework for CPTESs that incorporates integrated demand responses (IDRs) and EVs battery state-of-charge (SOC). In the ETN, a multiperiod traffic assignment model with time-shiftable traffic demands (MTA-TSTD) is established to optimize travelers' routes and departure times while capturing traffic flow distribution. Meanwhile, effective path generation models with EVs battery SOC are proposed to optimize charging energy during driving and construct the effective path sets for MTA-TSTD. In the PDN, a multiperiod optimal power flow model with time-shiftable power demands (MOPF-TSPD) is formulated to schedule local generators and flexible power demands while calculating the power flow distribution. To enhance temporal and spatial coordination in CPTESs, a distributed coordinated operation model considering IDRs is proposed, aiming to optimize energy consumption, alleviate congestion, and ensure system safety. Finally, an adaptive effective path generation algorithm and an ETN–PDN interaction algorithm are devised to efficiently solve these models. Numerical results on two test systems validate the effectiveness of the proposed models and algorithms.

Keywords: electric vehicles; dynamic wireless charging; power-traffic network; demand response; flexible demands; mileage limitation; state of charge

Citation: Geng, L.; Sun, C.; Song, D.; Zhang, Z.; Wang, C.; Lu, Z. Collaborative Optimization Framework for Coupled Power and Transportation Energy Systems Incorporating Integrated Demand Responses and Electric Vehicle Battery State-of-Charge. *Energies* **2024**, *17*, 5234. https://doi.org/10.3390/en17205234

Academic Editors: Javier Contreras and Islam Safak Bayram

Received: 9 September 2024
Revised: 9 October 2024
Accepted: 19 October 2024
Published: 21 October 2024

1. Introduction

In recent years, the global pollution problem has intensified due to the increasing consumption of fossil fuels [1]. Traditional power systems, which predominantly rely on these fuels, are among the major energy consumers. However, integrating innovative technologies, such as renewable energy generation [2,3], can help reduce this dependency. Furthermore, the transportation sector represents another significant contributor to pollution. Electric vehicles (EVs) have emerged as a promising alternative to gasoline vehicles (GVs), offering a viable solution for decarbonizing transportation and addressing climate change. According to [4], global EV sales reached nearly 14 million in 2023, accounting for 18% of all cars sold, and are expected to exceed 40 million by 2030. In line with this trend, public charging infrastructures have seen significant expansion and are expected to account for one-third of the total electricity used for EV charging, approximately 170 TWh,

by 2030 [5]. The growing adoption of EVs and the expansion of related charging infrastructures have enhanced the interconnection between electrified transportation network (ETNs) and power distribution network (PDNs) [6]. On the one hand, some factors such as road topology, congestion, and traffic control measures within the ETN will impact EV drivers' travel decisions (including charging decisions and route choices). These decisions significantly affect the spatial and temporal distribution of charging loads, which further influences the safety and economy of PDNs. On the other hand, the location of charging infrastructures and marginal electricity prices (which reflect the operating conditions of PDNs) will affect EV drivers' charging decisions and route choices, thereby impacting traffic flow distribution and the efficiency of ETNs [7].

Furthermore, recent rapid advancement in dynamic wireless charging (DWC) technology [8,9] makes it possible for EVs to charge while in motion. Leveraging this unique charging method, numerous DWC projects have been implemented globally, with notable examples in the UK, Germany, and South Korea [10]. This technological breakthrough further enhances the spatial and temporal dynamics of EV charging operations, which promotes a deeper integration between ETN and PDN. However, the convenience of DWC may lead to EV drivers to charge their batteries while driving home, shifting the peak charging demand to the afternoon commuting hours (16:00–19:00), rather than the evening period (19:00–22:00), as seen with the traditional plug-in charging mode. In this scenario, the heavy traffic demand in ETN during the evening rush hour, combined with tremendous EV charging demand in PDN, could potentially lead to simultaneous congestion in both the ETN and PDN [11]. Therefore, it is essential to move away from the independent operation models of the power and transportation sectors and establish a coupled power and transportation energy systems (CPTES) to optimize the performance of both networks [12].

Based on the above background, research on the coordinated operation of ETNs and PDNs has become a widely discussed topic among researchers in recent years. This growing interest has led to a series of research efforts and studies aimed at exploring and optimizing the integration of these networks. In conventional plug-in charging mode, reference [13] optimized road tolls and electricity prices at charging stations to reduce power losses in PDNs and total travel time in ETNs. Reference [14] presented a holistic modeling framework to analyze and optimize the interdependent ETN and PDN, which used a multicommunity user equilibrium model and best-response decomposition algorithm to achieve network equilibrium. Reference [15] proposed a smart EV charging management system in coupled networks and investigated how elastic traffic demands respond to locational charging prices. Reference [16] introduced a bi-level framework optimized by deep reinforcement learning to coordinate EV charging services, enhancing network operation and renewable energy integration. Reference [17] developed a variational inequality-based pricing scheme to enhance the coordination of PDN and ETN, integrating distribution locational marginal prices and congestion tolls to maximize social welfare. Reference [18] considered the impact of PDN operation on the traffic equilibrium state and proposed a generalized user equilibrium (GUE) method for CPTES. Recently, reference [19] addressed unrealistic assumptions in previous studies and proposed a holistic pricing framework to manage the power-traffic flows at network equilibrium, aiming for the least-cost social optimum state with minimum extra user charges. However, the above studies considered only single-period operation based on static traffic assignment (STA) while ignoring the time-varying behavior of power and traffic demands, which is impractical. In this regard, reference [20] investigated the impact of time-shiftable traffic demands on congestion alleviation in coupled networks. Reference [21] employed the quasi-dynamic traffic flow model and proposed a multiperiod hierarchical optimization approach for bi-peak shaving and bi-ramp smoothing in the coupled networks. To further improve the accuracy of simulating traffic flow dynamics, reference [22] utilized a dynamic traffic assignment (DTA) model to describe the dynamic propagation of traffic flow on conventional road segments, revealing the differences in simulation accuracy between STA, semidynamic traffic assignment (SDTA), and DTA models and their impact on adjustment results. Unlike reference [22], which calculated travel

times on road using predefined function expressions (such as the Bureau of Public Roads function), reference [23] proposed a dynamic traffic model with point queues to describe the spatial and temporal evolution of traffic flows that is congruent with established user equilibrium choices.

From the above-discussed research, great progress has been made in achieving coordination of CPTES under traditional plug-in charging modes. Next, we will explore the research advancements in the context of DWC mode. Reference [24] determined the optimal prices of both electricity and roads to maximize social welfare, and proposed first-best and second-best pricing models under different authoritarian regimes. Reference [25] proposed a decentralized framework to address traffic assignments in ETN as well as economic dispatch in PDN. Reference [26] mentioned that an independent system operator is authorized to manage generation assets and impose congestion tolls on electrified roads and designed an optimal traffic-power flow model to study the operational equilibria in coupled networks. Building on the work of [26], reference [11] addressed the temporal relationship of traffic demands by proposing an optimal power and semidynamic traffic flow model. This model was used to conduct congestion analysis over an entire day in coupled networks. Furthermore, reference [12] considered the shift in EVs charging demand from residential plug-in charging to charging-while-driving during commuting hours under the DWC mode, and proposed a bi-level integrated demand response framework to alleviate congestion in the coupled network. Reference [27] accurately depicted the time-varying electricity and traffic demands and proposed a coordinated optimization method for real and reactive power in coupled network. Different from the above studies that disregard the uncertainty of traffic demand and stochastic routing behavior of travelers, reference [28] considered the PDN load perturbation caused by the traffic demand uncertainty and proposed a robust dispatch method for coupled network. Reference [29] explored stochastic routing behavior of travelers and proposed a hybrid stochastic user equilibrium/information gap decision theory approach for the coordinated operation of coupled network.

The above-discussed studies provided a solid foundation for supporting the coordinated operation of ETNs and PDNs. However, the following inadequacies are identified through comparison.

1. The EVs battery state-of-charge (SOC) and differentiated charging energy for EVs with rigid charging demand during driving are not considered and modeled. Most existing studies often oversimplify the modeling of the ETN by assuming that all EVs can reach any charging station within the ETN to recharge and that they have the same and constant charging energy. These models overlook the differentiated charging energy and the range anxiety of EV drivers due to battery technology limitations. In practice, both current charging prices and SOC will remarkably impact EV recharging behavior while driving. For instance, EV drivers must ensure their battery does not run out when selecting a recharging path. Moreover, incentives related to charging may lead drivers to partially recharge their batteries rather than fully. Consequently, EVs traveling different routes between origin and destination (OD) pairs will experience varying energy demands due to differences in charging prices and SOC. In these cases, differentiated road charging prices may be an effective method for regulating the charging energy and route choices of travelers simultaneously.
2. Demand flexibility in both ETNs and PDNs is not fully exploited and modeled in the current literature. Most of the existing studies often regard both traffic and regular power demand to be nonshiftable over time, remaining constant across all scheduling horizons. Although these studies can achieve coordinated operation of CPTES by merely regulating the route choices of travelers, they may not effectively alleviate congestion within CPTES and can sometimes exacerbate congestion in the ETN. In practice, the traffic demands exhibit time-shiftability and can be influenced by factors such as traffic delays or charging costs. For example, when faced with excessively high charging prices or heavy traffic conditions, certain travelers may advance or postpone their departure times. Similarly, in the PDN, regular power demand is

also time-shiftable and can response to fluctuations in electricity prices. If the time-shiftable flexibility of both traffic and power demands is fully exploited, it may offer opportunities for more effectively alleviating congestion in CPTES.

3. Given the above two gaps, they still lack a more detailed model framework and effective management strategy for CPTES in response to range anxiety of EV drivers due to battery technology limitations (battery SOC), differentiated charging energy, and the flexibility of traffic and power demands. Determining how to maximize the social profit by tapping the flexibility of both networks while alleviating congestion is still an open question.

The present work addresses the inadequacies of past work by developing a collaborative optimization framework for CPTES, which incorporates IDRs and EV battery SOC. Specifically, it introduces the concept of integrated demand responses (IDRs) into the interdisciplinary studies between ETNs and PDNs, considers the range anxiety of EV drivers (EV battery SOC) in the ETN model, and proposes a distributed coordinated operation method to capture the interactions among transportation system operator (TSO), distribution system operator (DSO), and IDRs. The main contributions are twofold.

1. We develop two multiperiod models with demand flexibility for an ETN and a PDN, respectively. In the ETN, a multiperiod traffic assignment model with time-shiftable traffic demands (MTA-TSTD) is established to optimize travelers' routes and departure times while capturing traffic flow distribution. Additionality, effective path generation models with EV battery SOC are specifically designed to consider the range anxiety of EV drivers due to battery technology limitations, optimized differentiated charging energy of EVs, and construction of the effective path sets for MTA-TSTD. In the PDN, a multiperiod optimal power flow model with time-shiftable power demands (MOPF-TSPD) is formulated to schedule local generators and flexible power demands while calculating the power flow distribution.
2. Faced with the flexible response behavior of traffic and regular power demands demonstrated by the above models, we propose a distributed coordinated operation model considering IDRs for CPTES to maximize the social profit while alleviating congestion and ensure data privacy between the PDN and the ETN. An adaptive effective path generation algorithm is devised to solve MTA-TSTD models, which iteratively recognizes a subset of paths that are most likely taken. In addition, a TSO-DSO interaction algorithm is designed for alleviating congestion and ensuring data privacy between the PDN and ETN.

2. Model Formulation

Before detailing the mathematical model, we summarize the following two major assumptions made in the present work:

Assumption 1: *All devices within the CPTES are equipped with Internet of Things (IoT) capabilities, enabling effective data exchange and communication across different components of the system.*

Assumption 2: *Traffic and regular power users are incentivized to participate in IDR programs through financial rewards or discounts, making the participation process attractive and beneficial.*

2.1. Overall Framework

Figure 1 depicts the interaction among the TSO, DSO, and IDRs (flexible traffic and regular power demands). This interaction aims to promote the coordinated operation of CPTES from both temporal and spatial perspectives through IDRs, optimizing energy consumption to alleviate congestion and ensure system safety. Note that the TSO or DSO have no access to each other's network information when making decisions, which ensures data privacy for both networks. Each network optimizes its operations locally based on shared operational signals (e.g., charging price signals and charging power demand)

without direct access to each other's detailed datasets. Sensitive data from each network (e.g., vehicle information, network information of ETN and network information of PDN) remain within its respective system. Coordination occurs through anonymized aggregate data exchange rather than sharing detailed individual data, thus maintaining operational efficiency without compromising privacy. The specific interaction process is as follows.

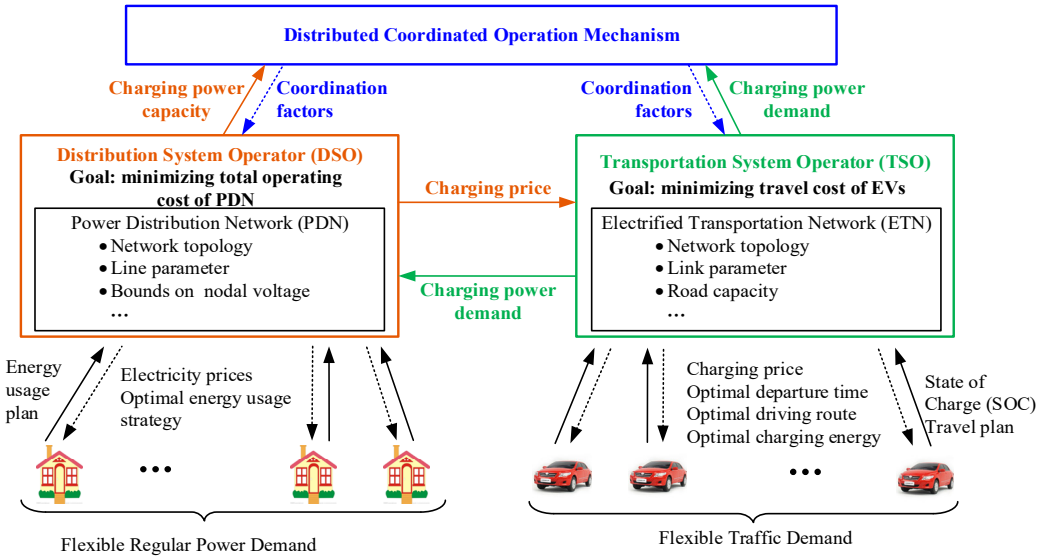

Figure 1. Collaborative optimization framework considering IDRs for CPTES.

In the ETN, the TSO has access to the network information of ETN, including network topology, link parameter, and road capacity. Each traveler must report their travel plan (including origin, destination, and departure time) and SOC to the TSO. Based on the $P^{\mathrm{T}}_{\mathrm{Lc},s,t} - update$ subproblem 1 (related to the MTA-TSTD model), the TSO reacts to charging prices, traffic conditions, and coordination factor, and accordingly determines the optimal route choices, departure times, recharging strategies (charging energy of each charging road along the driving path) for flexible travelers to minimize their travel costs.

In the PDN, the DSO has access to the network information of PDN, including network topology, line parameters, upper and lower bounds on nodal voltages, and so on. Each flexible regular power user must report their energy usage plan to the DSO. After validating the equivalent charging power demand at each DWC station through smart meters, the DSO determines optimal energy usage strategy for flexible regular power users, scheduling plan for local generators, charging power capacity, marginal charging prices, and regular electricity prices to minimize the total operational cost of PDN, based on the $P^{\mathrm{E}}_{\mathrm{Lc},s,t} - update$ subproblem 2 (related to the MOPF-TSPD model).

The distributed coordinated operation mechanism will receive the charging power demand and charging power capacity, update coordination factors, and then return them to the TSO and DSO. The TSO and DSO should reschedule and resubmit the charging power demand plans and charging power capacity until the convergence conditions are met.

2.2. Modeling of the ETN

Before detailing the mathematical model, we declare the following two premises: (1) The CPTES comprises the ETN and PDN, which are interconnected through wireless charging stations (roads) and mobile EVs. When EVs battery need to be recharged, DWC systems can continuously recharge them through designated charging lanes installed on roadways. (2) EVs in ETN are categorized into two types: some of them need battery recharge, and others do not need battery recharge. For EVs without recharging demand, we believe that the remaining capacity of EV batteries is sufficient to reach their destination, and the battery status information is not considered in ETN modeling. To distinguish them, EVs with recharging demand are referred to EVs, while those without recharging demand

are called GVs in the following description because they share a common route selection criterion with GVs.

2.2.1. Multiperiod Traffic Assignment Model with Time-Shiftable Traffic Demands

1. Travel time model

Travel time is a major consideration for travelers when selecting their routes and it is influenced by the congestion levels of the roads along the path. In ETN modeling, the congestion level of each road is typically quantified by Bureau of Public Roads (BPR) function [30] to describe the relationship between road travel time $\chi_a^t(\psi_a^t)$ and road flow ψ_a^t.

$$\chi_a^t(\psi_a^t) = \chi_a^0\left[1 + 0.15\left(\frac{\psi_a^t}{C_a}\right)^4\right], \quad \forall a \in \Omega_A, t \in \Omega_T \tag{1}$$

where χ_a^0 represents free flow travel time on road a. Notation C_a denotes the flow capacity of road a. The symbol Ω_A represents the set of roads in an ETN. Superscript t indicates time interval and Ω_T denotes the set of scheduling periods.

Each path is defined by a set of roads, with this relationship captured using an indicator variable. If a particular road is included in the path, the variable is set to 1, otherwise, it is set to 0. It is noteworthy that this indicator variable is predetermined and provided in advance based on the effective paths. In our work, the effective path sets $\Omega_{KGV,t}$ and $\Omega_{KEV,t}$ for GVs and EVs are determined by the effective path generation models with EV battery SOC, detailed in Section 2.2.2. Given the road travel time $\chi_a^t(\psi_a^t)$, the travel time $\tau_{GV,kg,w}^t$ of each effective path kg for GVs between each OD pair w can be calculated using Equation (2). Similarly, the travel time $\tau_{EV,ke,w}^t$ of each effective path ke for EVs can be calculated using Equation (3).

$$\tau_{GV,kg,w}^t = \sum_{a\in\Omega_A} \chi_a^t(\psi_a^t) x_{a,kg,w}^t, \quad \forall kg \in \Omega_{KGV,t}, w \in \Omega_{OD,t}, t \in \Omega_T \tag{2}$$

$$\tau_{EV,ke,w}^t = \sum_{a\in\Omega_A} \chi_a^t(\psi_a^t) x_{a,ke,w}^t, \quad \forall ke \in \Omega_{KEV,t}, w \in \Omega_{OD,t}, t \in \Omega_T \tag{3}$$

where $x_{a,kg,w}^t$ and $x_{a,ke,w}^t$ are indicator variables of effective path for GVs and EVs, respectively. Symbols $\Omega_{KGV,t}$ and $\Omega_{KEV,t}$ denote set of effective paths, respectively. $\Omega_{OD,t}$ represents set of all travel OD pairs in ETN.

2. Travel cost model

The total travel cost $\zeta_{GV,kg,w}^t$ for a GV driver on an effective path kg can be expressed as Equation (4), while for a single EV experienced on effective path ke, the path travel cost $\zeta_{EV,ke,w}^t$ becomes the summation of the travel time cost and charging cost, as detailed in Equation (5).

$$\zeta_{GV,kg,w}^t = \sum_{a\in\Omega_A} \eta\chi_a^t(\psi_a^t) x_{a,kg,w}^t, \quad \forall kg \in \Omega_{KGV,t}, w \in \Omega_{OD,t}, t \in \Omega_T \tag{4}$$

$$\zeta_{EV,ke,w}^t = \sum_{a\in\Omega_A} \eta\chi_a^t(\psi_a^t) x_{a,ke,w}^t + \sum_{a\in\Omega_A} \lambda_{a\in s\in j}^t E_{a,ke,w}^t, \quad \forall ke \in \Omega_{KEV,t}, w \in \Omega_{OD,t}, t \in \Omega_T \tag{5}$$

where η represents value of time, nominally valued at USD 10/hour. The term $\lambda_{a\in s\in j}^t$ refers to the charging electricity price of road a, specifically a node marginal electricity price at PDN bus j, which provides power to the DWC station s. Additionally, $E_{a,ke,w}^t$ denotes charging energy when an effective path ke between the OD pair w traverses road a. This quantity is optimized by the proposed effective path generation model for EVs.

3. Traffic flow model

Traffic flow models are developed to ensure traffic flow conservation in ETN. Specifically, the total traffic demand for each travel OD pair should equal the sum of traffic flows on all effective paths for that OD pair. Equations (6) and (7) balance the sum of path flows and the corresponding traffic demand.

$$\sum_{kg \in \Omega_{\mathrm{KGV},w,t}} H^t_{\mathrm{GV},kg,w} = q^t_{\mathrm{GV},w}, \quad \forall w \in \Omega_{\mathrm{OD},t}, t \in \Omega_T \tag{6}$$

$$\sum_{ke \in \Omega_{\mathrm{KEV},w,t}} H^t_{\mathrm{EV},ke,w} = q^t_{\mathrm{EV},w}, \quad \forall w \in \Omega_{\mathrm{OD},t}, t \in \Omega_T \tag{7}$$

where $q^t_{\mathrm{GV},w}/q^t_{\mathrm{EV},w}$ denotes the actual traffic demand of GVs/EVs between the travel OD pair w during the time period t, which will be explained in detail in the following time-shiftable traffic demands model.$H^t_{\mathrm{GV},kg,w}/H^t_{\mathrm{EV},ke,w}$ represents traffic flow of GVs/EVs on effective path kg/ke between travel OD pair w, and it must comply with the nonnegativity constraints outlined in (8) and (9).

$$H^t_{\mathrm{GV},kg,w} \geq 0, \quad \forall kg \in \Omega_{\mathrm{KGV},w,t}, w \in \Omega_{\mathrm{OD},t}, t \in \Omega_T \tag{8}$$

$$H^t_{\mathrm{EV},ke,w} \geq 0, \quad \forall ke \in \Omega_{KEV,w,t}, w \in \Omega_{\mathrm{OD},t}, t \in \Omega_T \tag{9}$$

The total traffic flow ψ^t_a on any road a is equal to the sum of the traffic flows from all effective paths for GVs and EVs that traverse the road a. Equations (10)–(12) describe the relationship between path flows and road flows.

$$\psi^t_{\mathrm{GV},a} = \sum_{w \in \Omega_{\mathrm{OD}}} \sum_{kg \in \Omega_{\mathrm{KGV}}} H^t_{\mathrm{GV},kg,w} x^t_{a,kg,w}, \quad \forall a \in \Omega_{\mathrm{A}},\ t \in \Omega_{\mathrm{T}} \tag{10}$$

$$\psi^t_{\mathrm{EV},a} = \sum_{w \in \Omega_{\mathrm{OD},t}} \sum_{ke \in \Omega_{\mathrm{KEV},t}} H^t_{\mathrm{EV},ke,w} x^t_{a,ke,w}, \quad \forall a \in \Omega_{\mathrm{A}},\ t \in \Omega_{\mathrm{T}} \tag{11}$$

$$\psi^t_a = \psi^t_{\mathrm{EV},a} + \psi^t_{\mathrm{GV},a}, \quad \forall a \in \Omega_{\mathrm{A}},\ t \in \Omega_{\mathrm{T}} \tag{12}$$

where $\psi^t_{\mathrm{GV},a}$ and $\psi^t_{\mathrm{EV},a}$ represent traffic flow of GVs and EVs on road a, respectively.

4. Time-shiftable traffic demands model

In transportation engineering, traffic demand refers to the number of vehicles traveling from an origin to a destination within a specific time period, which is a known constant and also called a trip rate. However, when faced with excessively high charging prices or heavy traffic conditions, certain travelers would rather postpone their travel to a less congested period, while some could advance their travel, exhibiting time-shiftability. To capture such temporal flexibility, traffic demand is modeled as a variable, which leads to the development of a time-shiftable traffic demands model. The detailed modeling process is as follows:

First, an elasticity coefficient ε is introduced to define the maximum transferable rate of traffic demand between each time period. Specifically, $\varepsilon_{t\tau}$ represents the maximum transferable rate at which traffic demand from current time period t can be shifted to time period τ. If t is less than τ, it indicates a delay in departure time; if t is greater than τ, it indicates an advance in departure time. Additionally, ε_{tt} represents the minimum nontransferable rate of traffic demand in the current time period t. For an ETN with T time periods during peak hours, the elasticity coefficients between time periods can be arranged into an $T \times T$ elasticity coefficient matrix, which can be represented as Equation (13):

$$E = \begin{bmatrix} \varepsilon_{11} & \varepsilon_{12} & \cdots & \varepsilon_{1T} \\ \varepsilon_{21} & \varepsilon_{22} & \cdots & \varepsilon_{2T} \\ \vdots & \vdots & \ddots & \vdots \\ \varepsilon_{T1} & \varepsilon_{T2} & \cdots & \varepsilon_{TT} \end{bmatrix} \tag{13}$$

Using the aforementioned elasticity coefficient matrix, the maximum transferable traffic demand $\overline{q}^{t\tau}_{\max,w}$ and the minimum nontransferable traffic demand $\overline{q}^{tt}_{\min,w}$ for each OD pair from the current time period t to other time periods τ can be expressed as Equations (14) and (15), respectively.

$$\overline{q}^{t\tau}_{\max,w} = \varepsilon_{t\tau}\overline{q}^{t}_{w}, \quad \forall t \neq \tau \in \Omega_{\mathrm{T}}, w \in \Omega_{\mathrm{OD},t} \tag{14}$$

$$\overline{q}^{tt}_{\min,w} = \varepsilon_{tt}\overline{q}^{t}_{w}, \quad \forall t \in \Omega_{\mathrm{T}}, w \in \Omega_{\mathrm{OD},t} \tag{15}$$

where $\overline{q}^{t}_{w}$ represents the initial traffic demand between the travel OD pair w during time period t.

Notice that if a driver could delay his travel from current period t to period τ, then he would also start his travel at an earlier period d for $t < d < \tau$. For the same reason, if a driver could advance his travel from period t to period τ, then he would also start at any period d for $\tau < d < t$. Therefore, the actual traffic demand from period t delay to period τ can be at most the sum of the maximum transferable traffic demand from period t to any period greater than τ. Similarly, the actual traffic demand from period t advance to period τ can be at most the sum of the maximum transferable traffic demand from period t to any period less than τ.

On this account, we introduce the decision variables $q^{t\tau}_{w}$ which stands for the actual number of vehicles that shift their travels from period t to period τ. Then, the time-shiftable traffic demand can be formulated by constraints (16)–(20).

$$q^{t\tau}_{w} \leq \sum_{k \geq \tau \in \Omega_{\mathrm{T}}} \overline{q}^{tk}_{\max,w}, \quad \forall t < \tau \in \Omega_{\mathrm{T}}, \forall w \in \Omega_{\mathrm{OD},t} \tag{16}$$

$$q^{t\tau}_{w} \leq \sum_{k \leq \tau \in \Omega_{\mathrm{T}}} \overline{q}^{tk}_{\max,w}, \quad \forall t > \tau \in \Omega_{\mathrm{T}}, \forall w \in \Omega_{\mathrm{OD},t} \tag{17}$$

$$q^{tt}_{w} \geq \overline{q}^{tt}_{\min,w}, \quad \forall t \in \Omega_{\mathrm{T}}, \forall w \in \Omega_{\mathrm{OD},t} \tag{18}$$

$$\sum_{\tau \in \Omega_{\mathrm{T}} \& \tau \neq t} q^{t\tau}_{w} + q^{tt}_{w} = \overline{q}^{t}_{w}, \quad \forall t \in \Omega_{\mathrm{T}}, \forall w \in \Omega_{\mathrm{OD},t} \tag{19}$$

$$\sum_{\tau \in \Omega_{\mathrm{T}} \& \tau \neq t} q^{\tau t}_{w} + q^{tt}_{w} = q^{t}_{w}, \quad \forall t \in \Omega_{\mathrm{T}}, \forall w \in \Omega_{\mathrm{OD},t} \tag{20}$$

where constraints (16)–(18) define the bounds on the actual transferred traffic demand. Equation (19) balances initial traffic demand $\overline{q}^{t}_{w}$ and the sum of traffic demand $q^{t\tau}_{w}$ transferred from the current period to other periods and nontransferred traffic demand remaining in the current period. Equation (20) balances actual traffic demand q^{t}_{w} and the sum of all traffic demand $q^{\tau t}_{w}$ transferred from other periods to the current period and nontransferred traffic demand q^{tt}_{w} remaining in the current period.

$$\begin{cases} q^{t\tau}_{\mathrm{GV},w} \leq \sum\limits_{k \geq \tau \in \Omega_{\mathrm{T}}} \overline{q}^{tk}_{\mathrm{GV},\max,w}, & \forall t < \tau \in \Omega_{\mathrm{T}}, \forall w \in \Omega_{\mathrm{OD},t} \\ q^{t\tau}_{\mathrm{GV},w} \leq \sum\limits_{k \leq \tau \in \Omega_{\mathrm{T}}} \overline{q}^{tk}_{\mathrm{GV},\max,w}, & \forall t > \tau \in \Omega_{\mathrm{T}}, \forall w \in \Omega_{\mathrm{OD},t} \\ q^{tt}_{\mathrm{GV},w} \geq \overline{q}^{tt}_{\mathrm{GV},\min,w}, & \forall t \in \Omega_{\mathrm{T}}, \forall w \in \Omega_{\mathrm{OD},t} \\ \sum\limits_{\tau \in \Omega_{\mathrm{T}} \& \tau \neq t} q^{t\tau}_{\mathrm{GV},w} + q^{tt}_{\mathrm{GV},w} = \overline{q}^{t}_{\mathrm{GV},w}, & \forall t \in \Omega_{\mathrm{T}}, \forall w \in \Omega_{\mathrm{OD},t} \\ \sum\limits_{\tau \in \Omega_{\mathrm{T}} \& \tau \neq t} q^{\tau t}_{\mathrm{GV},w} + q^{tt}_{\mathrm{GV},w} = q^{t}_{\mathrm{GV},w}, & \forall t \in \Omega_{\mathrm{T}}, \forall w \in \Omega_{\mathrm{OD},t} \end{cases} \tag{21}$$

$$\begin{cases} q_{\mathrm{EV},w}^{t\tau} \le \sum\limits_{k\ge\tau\in\Omega_{\mathrm{T}}} \overline{q}_{\mathrm{EV,max},w}^{tk}, & \forall t<\tau\in\Omega_{\mathrm{T}}, \forall w\in\Omega_{\mathrm{OD},t} \\ q_{\mathrm{EV},w}^{t\tau} \le \sum\limits_{k\le\tau\in\Omega_{\mathrm{T}}} \overline{q}_{\mathrm{EV,max},w}^{tk}, & \forall t>\tau\in\Omega_{\mathrm{T}}, \forall w\in\Omega_{\mathrm{OD},t} \\ q_{\mathrm{EV},w}^{tt} \ge \overline{q}_{\mathrm{EV,min},w}^{tt}, & \forall t\in\Omega_{\mathrm{T}}, \forall w\in\Omega_{\mathrm{OD},t} \\ \sum\limits_{\tau\in\Omega_{\mathrm{T}}\&\tau\ne t} q_{\mathrm{EV},w}^{t\tau} + q_{\mathrm{EV},w}^{tt} = \overline{q}_{\mathrm{EV},w}^{t}, & \forall t\in\Omega_{\mathrm{T}}, \forall w\in\Omega_{\mathrm{OD},t} \\ \sum\limits_{\tau\in\Omega_{\mathrm{T}}\&\tau\ne t} q_{\mathrm{EV},w}^{\tau t} + q_{\mathrm{EV},w}^{tt} = q_{\mathrm{EV},w}^{t}, & \forall t\in\Omega_{\mathrm{T}}, \forall w\in\Omega_{\mathrm{OD},t} \end{cases} \tag{22}$$

Keeping the above modeling ideas in mind, the time-shiftable traffic demand model for GVs and EVs can be expressed by constraints (21) and (22), respectively.

5. Mixed user equilibrium complementarity condition

Traffic assignment captures how vehicular flow is distributed throughout the ETN. Unlike a power system managed by a central operator, each driver in the ETN will choose the route that minimizes their own travel cost. Due to traffic congestion effect shown in (1), the shortest path may not always be the fastest one. The travel time on each road depends on the aggregated traffic flow on that link, which is influenced by the route choices of all EV and GV drivers. A steady state is achieved when no driver can reduce their travel cost by unilaterally changing their route, which is known Wardrop user equilibrium (UE) [30]. When the ETN reaches this equilibrium state, every utilized path kg/ke for each travel OD pair has an equal and minimal travel expense $\mu_{\mathrm{GV},w}^{t}/\mu_{\mathrm{EV},w}^{t}$, while the travel costs for unused paths exceed this minimum travel expense. This equilibrium state can be stated through the following nonlinear complementarity constraints.

$$0 \le H_{\mathrm{GV},kg,w}^{t} \perp \zeta_{\mathrm{GV},kg,w}^{t} - \mu_{\mathrm{GV},w}^{t} \ge 0, \quad \forall kg\in\Omega_{\mathrm{KGV},w,t}, w\in\Omega_{\mathrm{OD},t}, t\in\Omega_{\mathrm{T}} \tag{23}$$

$$0 \le H_{\mathrm{EV},ke,w}^{t} \perp \zeta_{\mathrm{EV},ke,w}^{t} - \mu_{\mathrm{EV},w}^{t} \ge 0, \quad \forall ke\in\Omega_{KEV,w,t}, w\in\Omega_{\mathrm{OD},t}, t\in\Omega_{\mathrm{T}} \tag{24}$$

where $0 \le a \perp b \ge 0$ stands for $a \ge 0$, $b \ge 0$ and $ab = 0$.

As demonstrated in [30], the Wardrop UE model can effectively capture traffic flow distribution and accurately represent route choices based on individual travel costs. It is also worth mentioning that the optimal route selections of individual travelers depend on the information they can gather. With advancements in communication technology, everyone now has easy access to real-time road conditions and regulatory policies. For example, navigation apps on smartphones can identify the best routes to a destination based on the latest information about congestion levels and charging prices of each road.

6. Multiperiod traffic assignment model with time-shiftable traffic demands

In summary, Equations (1)–(12) and (21)–(24) form MTA-TSTD. However, the complementary constraints presented in (23)–(24) deviate from standard constraint forms, making the MTA-TSTD difficult to solve. As noted in [31], the Wardrop UE condition aligns with the Karush–Kuhn–Tucker (KKT) optimality conditions of a convex optimization problem, specifically the Beckmann model. By extending the Beckmann model into a multiperiod framework, the MTA-TSTD is transformed into the following convex optimization problem.

$$\begin{aligned} &\min F_{\mathrm{MTA-TSTD}} = F_{\mathrm{DT}} + F_{\mathrm{CH}} \\ &\text{s.t.} \left\{ \begin{array}{c} (4)-(12) \\ (21)-(22) \end{array} \right\} \end{aligned} \tag{25}$$

where $F_{\mathrm{MTA-TSTD}}$ is objective function value. F_{DT} and F_{CH} represent the total delay cost for traffic users and the total charging cost for EVs over the entire scheduling cycle, as detailed in Equations (26) and (27), respectively.

$$F_{\mathrm{DT}} = \sum_{t\in\Omega_{\mathrm{T}}} \sum_{a\in\Omega_{\mathrm{A}}} \eta \int_0^{\psi_a^t} \chi_a^t(\psi_a^t)\, \mathrm{d}\psi_a^t = \sum_{t\in\Omega_{\mathrm{T}}} \sum_{a\in\Omega_{\mathrm{A}}} \eta\chi_a^0 \left[\psi_a^t + \frac{0.15\times(\psi_a^t)^5}{4\times(C_a)^4} \right] \tag{26}$$

$$\begin{aligned} F_{\mathrm{CH}} &= \sum_{t\in\Omega_{\mathrm{T}}}\sum_{w\in\Omega_{\mathrm{OD}}}\sum_{ke\in\Omega_{\mathrm{KEV},w}}\int_0^{H^t_{\mathrm{EV},ke,w}}\sum_{a\in\Omega_{\mathrm{A}}}\lambda^t_{a\in s\in j}E^t_{a,ke,w}\mathrm{d}H^t_{\mathrm{EV},ke,w} \\ &= \sum_{t\in\Omega_{\mathrm{T}}}\sum_{w\in\Omega_{\mathrm{OD}}}\sum_{ke\in\Omega_{\mathrm{KEV},w}}\left(\sum_{a\in\Omega_{\mathrm{A}}}\lambda^t_{a\in s\in j}E^t_{a,ke,w}\right)H^t_{\mathrm{EV},ke,w} \end{aligned} \tag{27}$$

Remark 1. *The above MTA-TSTD model is strictly convex optimization problem with linear constraints, and can be efficiently solved by nonlinear solvers such as IPOPT 3.14.4 (Interior Point OPTimizer, a software package for large-scale nonlinear optimization problems).*

2.2.2. Effective Path Generation Models with Battery SOC of EVs

Based on the description in Section 2.2.1, it is essential to determine the effective path sets Ω_{KEV} and Ω_{KGV} before solving the MTA-TSTD model. In most previous studies, path search algorithms were employed to enumerate sets of travel paths between each OD pair. While enumeration can generate all potential paths, many of these paths may not be selected by drivers, as they tend to choose the paths with the lowest travel costs. Consequently, many of the enumerated paths may be redundant, which significantly increases the computational complexity of the MTA-TSTD model.

Furthermore, the effective path generation for EVs involves additional complexities beyond those for GVs, including battery SOC and charging decisions (such as choosing DWC stations or roads and determining charging energy). This complexity makes enumeration methods particularly burdensome and potentially impractical for EV path analysis. To address these issues, we propose two types of effective path generation models to construct the effective path sets Ω_{KEV} and Ω_{KGV} for both EVs and GVs.

1. Effective path generation model for EVs

For an EV driver, the primary objectives are to maximize battery replenishment and minimize travel costs during their journey. To achieve these goals, the effective path generation model for EVs (EPGM-EVs) focuses on enhancing travel benefits of EV driver by identifying the optimal travel route and optimizing charging energy at DWC road along the route. This optimization considers and balances the current traffic flow distribution, battery SOC, and charging prices to improve the overall travel experience for the EV driver.

To characterize the charging behavior of EVs, we employ utility functions [32] from microeconomics for analysis and modeling. In practical ETN, EV drivers who select the same route tend to display similar charging behaviors. Thus, the utility function $\mathrm{U}^t_{\mathrm{EV},ke,w}$ for EV drivers on the same path can be standardized, and the following two essential properties need to be exhibited:

Property 1. *The charging utility function $\mathrm{U}^t_{\mathrm{EV},ke,w}(E^t_{a,ke,w},\omega)$ should be a nondecreasing function of the charging energy $E^t_{a,ke,w}$. As drivers generally aim to maximize their energy replenishment up to the allowable capacity, user satisfaction or utility increase with the amount of charging energy. When the charging energy $E^t_{a,ke,w}$ reaches the output maximum value L_a of DWC road, user satisfaction with the charging experience peaks.*

Property 2. *The charging marginal revenue $\partial\mathrm{U}^t_{\mathrm{EV},ke,w}(E^t_{a,ke,w},\omega)/\partial E^t_{a,ke,w}$ of EV drivers derived from additional charging energy should decrease as the total charging energy increases. Despite the increasing utility with more charging energy $E^t_{a,ke,w}$, the rate of additional benefit (marginal revenue) that EV drivers receive from each additional unit of charging decreases as the total charging energy increases. This results in a decreasing rate of added utility, reflecting that the utility approaches a saturation point, where further increases in charging energy yield progressively smaller gains.*

Considering the above two properties, we employ a widely used piecewise quadratic function to quantify the charging utility for EV drivers traversing charging roads. The detailed model is as follows:

$$U^t_{\mathrm{EV},a,ke,w}(E^t_{a,ke,w},\omega) = \begin{cases} E^t_{a,ke,w}(\omega - \frac{\alpha}{2}E^t_{a,ke,w}), & 0 \le E^t_{a,ke,w} \le \frac{\omega}{\alpha} \\ \frac{\omega^2}{2\alpha}, & E^t_{a,ke,w} \ge \frac{\omega}{\alpha} \end{cases} \tag{28}$$

where the symbol ω is a parameter in the charging utility function, representing the sensitivity of EV drivers to the charging prices. A higher value of ω indicates a stronger willingness of EV drivers to fully recharge their batteries, despite high cost. Notation α is a preset parameter influencing the peak value of the utility function. When variable $E^t_{a,ke,w}$ maps to the peak value of utility function, the charging road will deliver the maximum charging energy L_a, and then

$$\frac{\omega}{\alpha} = L_a \Rightarrow \alpha = \frac{\omega}{L_a} \tag{29}$$

The total charging utility function of EV drivers on the path ke between OD pair w is given by Equation (30):

$$\mathrm{U}^t_{\mathrm{EV},ke,w} = \sum_{a\in\Omega_\mathrm{A}} \left[\omega E^t_{a,ke,w} - \frac{\omega}{2L_a}(E^t_{a,ke,w})^2\right] \tag{30}$$

The total travel costs of EV drivers on the path ke between OD pair w is given by Equation (31):

$$\kappa^t_{\mathrm{EV},ke,w} = \sum_{a\in\Omega_\mathrm{A}} \left[\eta\chi^t_a(\psi_a)\gamma^t_{a,ke} + \lambda^t_{a\in s\in j}E^t_{a,ke,w}\right] \tag{31}$$

where $\kappa^t_{\mathrm{EV},ke,w}$ is the travel cost of EVs in path ke between OD pair w. $\gamma^t_{a,ke}$ is an 0–1 decision variable, and if the path ke includes road a, then $\gamma^t_{a,ke} = 1$, otherwise, $\gamma^t_{a,ke} = 0$.

Combining the above Equations (30) and (31), for each OD pair $w \in \Omega_{\mathrm{OD},t}$, the detailed EPGM-EVs can be described as follows.

- Objective function:

$$\max_{\boldsymbol{\gamma},\mathbf{E}} W^t_{\mathrm{EV},ke,w} = \mathrm{U}^t_{\mathrm{EV},ke,w} - \kappa^t_{\mathrm{EV},ke,w} \tag{32}$$

where $W^t_{\mathrm{EV},ke,w}$ is the travel benefit of EVs in path ke between OD pair w.

- Constraints:

$$\boldsymbol{\Delta\gamma}^t_{ke,w} = \mathbf{I}^t_{\mathrm{EV},w}\ \forall w \in \Omega_{\mathrm{OD},t},\ t \in \Omega_\mathrm{T} \tag{33}$$

$$\mathrm{SOC}^t_{i,ke,w} - d_a\varpi + E^t_{a,ke,w} - \mathrm{SOC}^t_{j,ke,w} = \varepsilon^t_{a,ke,w}\ \forall (i,j) = a \in \Omega_\mathrm{A},\ t \in \Omega_\mathrm{T} \tag{34}$$

$$\begin{cases} \varepsilon^t_{a,ke,w} \ge -\mathrm{M}\left(1-\gamma^t_{a,ke,w}\right) \\ \varepsilon^t_{a,ke,w} \le \mathrm{M}\left(1-\gamma^t_{a,ke,w}\right) \end{cases} \forall (i,j) = a \in \Omega_\mathrm{A}, t \in \Omega_\mathrm{T} \tag{35}$$

$$\mathrm{SOC}^t_{i,ke,w} - d_a\varpi + E^t_{a,ke,w} \ge -\mathrm{M}\left(1-\gamma^t_{a,ke,w}\right) + m\ \forall (i,j) = a \in \Omega_\mathrm{A}, t \in \Omega_\mathrm{T} \tag{36}$$

$$\mathrm{SOC}^t_{i,ke,w} - d_a\varpi + E^t_{a,ke,w} \le \mathrm{M}\left(1-\gamma^t_{a,ke,w}\right) + \mathrm{SOC}_\mathrm{max}\ \forall (i,j) = a \in \Omega_\mathrm{A}, t \in \Omega_\mathrm{T} \tag{37}$$

$$\begin{cases} 0 \le E^t_{a,ke,w} \le L_a\gamma^t_{a,ke,w} & \text{if } a \in s \in \Omega_\mathrm{WCS} \\ E^t_{a,ke,w} = 0 & \text{if } a \notin s \in \Omega_\mathrm{WCS} \end{cases}, \forall t \in \Omega_\mathrm{T} \tag{38}$$

$$\mathrm{SOC}^t_{r,ke,w} = \mathrm{SOC}_{\mathrm{ini},w},\ \forall t \in \Omega_\mathrm{T} \tag{39}$$

$$\mathrm{SOC}_{\mathrm{end},w} \le \mathrm{SOC}^t_{s,ke,w} \le \mathrm{SOC}_\mathrm{max},\ \forall t \in \Omega_\mathrm{T} \tag{40}$$

Equation (33) constrains all possible paths between each OD pair. The node-link incidence matrix Δ depicts the network topology, where each column corresponds to a road and contains two nonzero elements: 1 and -1 at the positions related to the entrance and exit nodes, respectively. In view of the definition of Δ, $\boldsymbol{\gamma}^t_{ke,w}$ represents a chain of connected roads from origin r and travels to its destination s. $\mathbf{I}^t_{\mathrm{EV},w}$ has two nonzero elements, 1 and -1 at the entries corresponding to the origin node r and the destination node s. Constraints (34) and (35) describe the variation in battery charge experienced by an EV traveling through any road. $\mathrm{SOC}^t_{i,ke,w}$ and $\mathrm{SOC}^t_{j,ke,w}$ represent the initial and final SOC, respectively, for the EV when it travels through the road on a path ke between OD pair w. Notations d_a and ϖ denote the road distance and driving energy consumption rate of EVs, respectively. The symbols $\varepsilon^t_{a,ke,w}$ and M are auxiliary variable and infinite constant. Constraints (36) and (37) take into account the impact of range limitations and battery capacity of EVs. When an EV traverses a certain road and reaches the next node, the SOC must remain above a minimum threshold m and below the maximum capacity $\mathrm{SOC}_{\max}$. Constraints (38) specify that if a path includes a DWC road, the charging energy $E^t_{a,ke,w}$ on that road must be less than the maximum allowable amount L_a; otherwise, $E^t_{a,ke,w}$ is set to zero. Ω_{WCS} denotes the set of DWC stations in ETN. Constraints (39) and (40) indicate that the EV must meet the initial and final SOC requirements. $\mathrm{SOC}_{\mathrm{ini},w}$ and $\mathrm{SOC}_{\mathrm{end},w}$ denote the SOCs of the EV at the origin r and at the destination s, respectively.

2. Effective path generation model for GVs

For a GV driver, the primary objectives are to minimize travel costs during their journey, without the need for recharging. Therefore, the effective path generation model for GVs (EPGM-GVs) is relatively straightforward, as it does not require optimizing charging energy or considering battery state of charge (SOC) constraints. This model is described as follows:

$$\min \kappa^t_{\mathrm{GV},kg,w} = \sum_{a \in \Omega_{\mathrm{A}}} \eta \chi^t_a(\psi^t_a) \gamma^t_{a,kg} \tag{41}$$

$$\Delta \boldsymbol{\gamma}^t_{kg} = \mathbf{I}^t_{\mathrm{GV},w} \; \forall w \in \Omega_{\mathrm{OD},t}, t \in \Omega_{\mathrm{T}} \tag{42}$$

2.3. Modeling of PDN

2.3.1. Demand–Price Elasticity Model

The response of regular power demand to market electricity prices is typically described using a demand–price elasticity model. This model guides regular power users to adjust their power demand in response to real-time price changes, thereby improving the operational characteristics of the PDN during peak periods. The specific modeling process is as follows.

In actual electricity usage, a user's power demand during a given period is influenced not only by the current period's electricity price but also by the prices of other periods. To describe the interrelationship between electricity prices and power demand across different periods, the demand–price elasticity model defines two distinct elasticity coefficients: the self-elasticity coefficient e_{tt} and the cross-elasticity coefficient $e_{t\tau}$ [33].

$$e_{tt} = \frac{\xi^t_{\mathrm{ini}}}{P^t_{\mathrm{Ld,ini}}} \frac{\partial P^t_{\mathrm{Ld}}}{\partial \xi^t}, \quad \forall t \in \Omega_{\mathrm{T}} \tag{43}$$

$$e_{t\tau} = \frac{\xi^\tau_{\mathrm{ini}}}{P^t_{\mathrm{Ld,ini}}} \frac{\partial P^t_{\mathrm{Ld}}}{\partial \xi^\tau}, \quad \forall \tau \neq t \in \Omega_{\mathrm{T}} \tag{44}$$

where $P^t_{\mathrm{Ld,ini}}$ and P^t_{Ld} represent the initial power demand and the power demand after price response for regular power users during period t, respectively. ξ^t_{ini} and ξ^t represent the initial electricity price and the price after demand response for period t, respectively.

After implementing demand response, the regular power user's energy demand at any given period t should be optimized to maximize net benefits WE, defined as the difference

between the revenue from electricity consumption $W(P_{\mathrm{Ld}}^t)$ and the cost of purchasing electricity $\xi^t P_{\mathrm{Ld}}^t$, given by

$$WE = W(P_{\mathrm{Ld}}^t) - \xi^t P_{\mathrm{Ld}}^t, \quad \forall t \in \Omega_{\mathrm{T}} \tag{45}$$

When the regular power user responds to the market electricity price in the current period t, the revenue function from electricity consumption can be expressed as

$$W(P_{\mathrm{Ld}}^t) = W\left(P_{\mathrm{Ld,ini}}^t\right) - \xi_{\mathrm{ini}}^t\left(P_{\mathrm{Ld}}^t - P_{\mathrm{Ld,ini}}^t\right)\left(1 + \frac{P^t - P_{\mathrm{Ld,ini}}^t}{2e_{tt}P_{\mathrm{Ld,ini}}^t}\right), \quad \forall t \in \Omega_{\mathrm{T}} \tag{46}$$

We substitute Equation (46) into Equation (45) and compute the differential equation for Equation (45) with respect to the current period's power demand P_{Ld}^t. When $\partial WE/\partial P_{\mathrm{Ld}}^t = 0$, the regular power user's net benefits are maximized. The resulting power demand in response to changes in the electricity price during the current period t can be expressed as

$$P_{\mathrm{Ld}}^t = P_{\mathrm{Ld,ini}}^t + P_{\mathrm{Ld,ini}}^t e_{tt}\left(\frac{\xi^t - \xi_{\mathrm{ini}}^t}{\xi_{\mathrm{ini}}^t}\right), \quad \forall t \in \Omega_{\mathrm{T}} \tag{47}$$

Using a method similar to that in Equation (47), the regular power demand that maximizes the user's net benefits in response to changes in electricity prices during other periods can be expressed as

$$P_{\mathrm{Ld}}^t = P_{\mathrm{Ld,ini}}^t + P_{\mathrm{Ld,ini}}^t \sum_{\tau \in \Omega_{\mathrm{T}} \& \tau \neq t} e_{\tau t}\left(\frac{\xi^\tau - \xi_{\mathrm{ini}}^\tau}{\xi_{\mathrm{ini}}^\tau}\right), \quad \forall t \in \Omega_{\mathrm{T}} \tag{48}$$

By combining Equations (47) and (48), the total power demand that maximizes the user's net benefits can be expressed as

$$\begin{aligned} P_{\mathrm{Ld}}^t &= P_{\mathrm{Ld,ini}}^t + \left[P_{\mathrm{Ld,ini}}^t e_{tt}\left(\frac{\xi^t - \xi_{\mathrm{ini}}^t}{\xi_{\mathrm{ini}}^t}\right) + P_{\mathrm{Ld,ini}}^t \sum_{\tau \in \Omega_{\mathrm{T}} \& \tau \neq t} e_{\tau t}\left(\frac{\xi^\tau - \xi_{\mathrm{ini}}^\tau}{\rho_{\mathrm{ini}}^\tau}\right)\right] \\ &= P_{\mathrm{Ld,ini}}^t + \Delta P_{\mathrm{Ld}}^t, \quad \forall t \in \Omega_{\mathrm{T}} \end{aligned} \tag{49}$$

where ΔP_{Ld}^t represents the change of regular power demand after participating in demand response.

2.3.2. Multiperiod Optimal Power Flow Model with Time-Shiftable Power Demands

1. Objective function

The objective function of the MOPF-TSPD is to minimize the total operational cost over the scheduling period $F_{\mathrm{MOPF-TSPD}}$, which includes the purchasing electricity cost from the main grid F_{sub}, the generation cost F_{G}, and the penalty cost for load peak–valley differences $F_{\mathrm{peak-Valley}}$.

$$\min F_{\mathrm{MOPF-TSPD}} = F_{\mathrm{sub}} + F_{\mathrm{G}} + F_{\mathrm{peak-Valley}} \tag{50}$$

$$F_{\mathrm{sub}} = \rho_{\mathrm{sub}}^t \sum_{t \in \Omega_{\mathrm{T}}} \sum_{j \in \Omega_{\mathrm{sub}}} P_{\mathrm{sub},j}^t \tag{51}$$

$$F_{\mathrm{G}} = \sum_{t \in \Omega_{\mathrm{T}}} \sum_{g \in \Omega_{\mathrm{G}}} \left[a_g (P_{\mathrm{G},g}^t)^2 + b_g P_{\mathrm{G},g}^t\right] \tag{52}$$

$$F_{\mathrm{peak-Valley}} = \rho_{\mathrm{peak-Valley}}\left[P_{\mathrm{L}}^{\max} - P_{\mathrm{L}}^{\min}\right] \tag{53}$$

$$P_{\mathrm{L}}^t = \sum_{j \in \Omega_{\mathrm{N}}} P_{\mathrm{Ld},j}^t + \sum_{j \in \Omega_{\mathrm{N}}} P_{\mathrm{Lc},j}^t, \quad \forall t \in \Omega_{\mathrm{T}} \tag{54}$$

$$\begin{cases} P_{\mathrm{L}}^{\max} = \max\left(P_{\mathrm{L}}^{t}\right) \\ P_{\mathrm{L}}^{\min} = \min\left(P_{\mathrm{L}}^{t}\right) \end{cases} \tag{55}$$

where ρ_{sub}^{t} represents the unit cost of purchasing electricity from the higher-level power grid. $P_{\mathrm{sub},j}^{t}$ denotes active power delivered through line connected to the slack bus. $P_{\mathrm{G},g}^{t}$ represents the active power of local generator. Notations a_g and b_g are production cost coefficients of the generator. The variables P_{L}^{t}, $P_{\mathrm{Ld},j}^{t}$, and $P_{\mathrm{Lc},j}^{t}$ represent the total system load, regular power load, and charging load at node j of the PDN during period t, respectively. The variables $P_{\mathrm{L}}^{\max}$ and $P_{\mathrm{L}}^{\min}$ represent the maximum and minimum values of the total system load during the scheduling period, respectively.

2. Constraints

The MOPF-TSPD is subjected to branch flow equations with second-order cone relaxation (SOC) [34,35], as shown in (56)–(60):

$$P_{i,j}^{t} + P_{\mathrm{G},j}^{t} - I_{i,j}^{t} r_{i,j} - \sum_{h \in \Omega_j} P_{j,h}^{t} - P_{\mathrm{L},j}^{t} = 0, \quad \forall (i,j) \in \Omega_{\mathrm{L}},\ t \in \Omega_{\mathrm{T}} \tag{56}$$

$$P_{\mathrm{L},j}^{t} = P_{\mathrm{Ld},j}^{t} + P_{\mathrm{Lc},j}^{t}, \quad \forall j \in \Omega_{\mathrm{N}},\ t \in \Omega_{\mathrm{T}} \tag{57}$$

$$Q_{i,j}^{t} + Q_{\mathrm{G},j}^{t} - I_{i,j}^{t} x_{i,j} - \sum_{h \in \Omega_j} Q_{j,h}^{t} - Q_{\mathrm{L},j}^{t} = 0, \quad \forall (i,j) \in \Omega_{\mathrm{L}},\ t \in \Omega_{\mathrm{T}} \tag{58}$$

$$U_{i}^{t} - U_{j}^{t} = 2\left(r_{i,j} P_{i,j}^{t} + x_{i,j} Q_{i,j}^{t}\right) - \left[(r_{i,j})^2 + (x_{i,j})^2\right] I_{i,j}^{t}, \quad \forall (i,j) \in \Omega_{\mathrm{L}},\ t \in \Omega_{\mathrm{T}} \tag{59}$$

$$\left\| \begin{matrix} 2P_{i,j}^{t} \\ 2Q_{i,j}^{t} \\ I_{i,j}^{t} - U_{i}^{t} \end{matrix} \right\| \leq I_{i,j}^{t} + U_{i}^{t}, \quad \forall (i,j) \in \Omega_{\mathrm{L}}, t \in \Omega_{\mathrm{T}} \tag{60}$$

$$\left(P_{i,j}^{t}\right)^2 + \left(Q_{i,j}^{t}\right)^2 \leq \left(S_{i,j}^{\max}\right)^2 \forall (i,j) \in \Omega_{\mathrm{L}}, t \in \Omega_{\mathrm{T}} \tag{61}$$

$$P_{i,j}^{t} - r_{i,j} I_{i,j}^{t} \geq 0 \ \forall (i,j) \in \Omega_{\mathrm{L}}, t \in \Omega_{\mathrm{T}} \tag{62}$$

$$Q_{i,j}^{t} - x_{i,j} I_{i,j}^{t} \geq 0 \ \forall (i,j) \in \Omega_{\mathrm{L}}, t \in \Omega_{\mathrm{T}} \tag{63}$$

$$U_{j}^{\min} \leq U_{j}^{t} \leq U_{j}^{\max} \ \forall j \in \Omega_{\mathrm{N}}, t \in \Omega_{\mathrm{T}} \tag{64}$$

where constraints (56) and (58) enforce active and reactive power balance at each PDN node, respectively. Constraints (59) link voltage drop to the power flow on each line. Constraints (60) indicate the SOC relaxation. Constraints (61)–(63) impose power flow limitations of distribution lines. Constraints (64) impose bounds on nodal voltages.$P_{i,j}^{t}$ and $Q_{i,j}^{t}$ are the active and reactive power of branch (i,j) at period t. $P_{j,h}^{t}$ and $Q_{j,h}^{t}$ are the active and reactive power of branch (j,h) connected to node j at period t. $r_{i,j}$ and $x_{i,j}$ are the resistance and reactance of branch (i,j). $P_{\mathrm{L},j}^{t}$ and $Q_{\mathrm{L},j}^{t}$ are the active and reactive power demand at node j at period t. $I_{i,j}^{t}$ and U_{j}^{t} represent squared current magnitude in branch (i,j) and squared voltage magnitude at node j at period t, respectively. $S_{i,j}^{\max}$ is maximum allowable capacity of distribution line (i,j). $U_{j}^{\min}$ and $U_{j}^{\max}$ are the minimum and maximum squared values of node voltage, respectively.

Assuming that all distributed energy sources in PDN are local generators, the generators in the multiperiod scheduling model must satisfy the ramp rate constraints, as shown in (65) to (67).

$$P_{\mathrm{G},g}^{\min} \leq P_{\mathrm{G},g}^{t} \leq P_{\mathrm{G},g}^{\max}, \quad \forall g \in \Omega_{\mathrm{G}},\ t \in \Omega_{\mathrm{T}} \tag{65}$$

$$Q_{\mathrm{G},g}^{\min} \leq Q_{\mathrm{G},g}^{t} \leq Q_{\mathrm{G},g}^{\max}, \quad \forall g \in \Omega_{\mathrm{G}},\ t \in \Omega_{\mathrm{T}} \tag{66}$$

$$-P_{\mathrm{G},g}^{\mathrm{ramp}} \leq P_{\mathrm{G},g}^{t} - P_{\mathrm{G},g}^{t-1} \leq P_{\mathrm{G},g}^{\mathrm{ramp}}, \quad \forall g \in \Omega_{\mathrm{G}},\ t \in \Omega_{\mathrm{T}} \tag{67}$$

where constraints (65) and (66) impose the upper/lower bound on generators output. $P_{G,g}^{ramp}$ represents the ramp rate limit of distributed generator.

To address unforeseen situations such as generator failures and load response errors, the PDN needs to provide a certain amount of upward and downward spinning reserves, as shown in (68) to (73).

$$0 \le s_{u,g}^{t} \le \min\left(P_{G,g}^{max} - P_{G,g}^{t}, P_{G,g}^{ramp}\right), \quad \forall g \in \Omega_G,\ t \in \Omega_T \tag{68}$$

$$0 \le s_{d,g}^{t} \le \min\left(P_{G,g}^{t} - P_{G,g}^{min}, P_{G,m}^{ramp}\right), \quad \forall g \in \Omega_G,\ t \in \Omega_T \tag{69}$$

$$S_{u}^{t} \ge \varepsilon_d \sum_{j \in \Omega_N} P_{L,j}^{t}, \quad \forall t \in \Omega_T \tag{70}$$

$$S_{d}^{t} \ge \varepsilon_d \sum_{j \in \Omega_N} P_{L,j}^{t}, \quad \forall\, t \in \Omega_T \tag{71}$$

$$S_{u}^{t} = \sum_{g \in \Omega_G} s_{u,g}^{t}, \quad \forall\, t \in \Omega_T \tag{72}$$

$$S_{d}^{t} = \sum_{g \in \Omega_G} s_{d,g}^{t}, \quad \forall\, t \in \Omega_T \tag{73}$$

where $s_{u,g}^{t}$ and $s_{d,g}^{t}$ denote upward and downward spinning reserves of distributed generator g at time period t. S_{u}^{t} and S_{d}^{t} represent upward and downward spinning reserves of the entire distribution system at time period t. ε_d indicates error coefficient of the regular power load participating in demand response.

For the demand–price elasticity model, it is necessary to limit the variation in electricity prices to a range acceptable to users. Additionally, as electricity prices change, only a portion of users may be willing to alter their consumption habits. Therefore, it is essential to ensure that user satisfaction remains above a certain threshold.

$$\begin{cases} \xi^{min} \le \xi^{t} \le \xi^{max} \\ D_s = 1 - \dfrac{\sum\limits_{t \in \Omega_T} \left|\Delta P_{Ld,j}^{t}\right|}{\sum\limits_{t \in \Omega_T} P_{Ld,j}^{t}} \ge 0.8 \end{cases} \tag{74}$$

where ξ^{min} and ξ^{max} denote the minimum and maximum electricity prices. D_s represents user satisfaction with their energy consumption patterns.

Remark 2. *The above MOPF-TSPD model is a second-order cone programming problem and can be effectively solved using CPLEX or Mosek solvers. CPLEX is an optimization solver developed by IBM that is widely used for linear programming, mixed-integer programming, and quadratic programming problems. Mosek is developed by Mosek ApS, a Danish company specializing in optimization software. It is capable of solving a variety of optimization problems, including linear programming, mixed-integer programming, and second-order cone programming.*

2.4. Distributed Coordinated Operation Model Considering IDR

Faced with the flexible response behavior of traffic and regular power demands demonstrated by the above MTA-TSTD and MOPF-TSPD models, we propose a distributed coordinated operation model considering IDRs for CPTES to maximize the social profit while alleviating congestion and ensure data privacy between the PDN and ETN. This model calculates the marginal electricity prices at nodes in the PDN for each period within the scheduling horizon and utilizes the spatiotemporal differences in these prices to adjust the spatiotemporal distribution of EV charging loads. Additionally, it sets real-time electricity prices to guide regular power loads in responding to price changes and modifying their energy consumption. Through IDRs, the

CPTES achieves coordinated operation on both temporal and spatial levels, thereby enhancing overall system efficiency and stability.

The established MTA-TSTD and MOPF-TSPD models are coupled through the load constraints of DWC stations, as represented by Equation (75):

$$\begin{aligned} P_{\mathrm{Lc},s,t} &= \sum_{a\in\Omega_{\mathrm{A}}}\sum_{w\in\Omega_{\mathrm{OD}}}\sum_{ke\in\Omega_{\mathrm{KEV},w,t}} H^{t}_{\mathrm{EV},ke,w}E^{t}_{a,ke,w} \\ P^{\mathrm{E}}_{\mathrm{Lc},s,t} &= P^{\mathrm{T}}_{\mathrm{Lc},s,t} \end{aligned} \qquad \forall s\in\Omega_{\mathrm{WCS}}, t\in\Omega_{\mathrm{T}} \tag{75}$$

Here, $P^{\mathrm{E}}_{\mathrm{Lc},s,t}$ and $P^{\mathrm{T}}_{\mathrm{Lc},s,t}$ represent the optimized charging loads obtained from the PDN and the ETN, respectively. Note that $P^{\mathrm{T}}_{\mathrm{Lc},s,t}$ refers to the charging power demand optimized by the TSO, while $P^{\mathrm{E}}_{\mathrm{Lc},s,t}$ denotes the charging power capacity optimized by the DSO.

Based on the alternating direction multiplier method (ADMM) [36], the coupling constraints (75) are relaxed by introducing the Lagrange multiplier $\rho_{s,t}$. This leads to the establishment of an augmented Lagrangian function for CPTES, as shown in Equation (76):

$$\begin{aligned} L(P^{\mathrm{T}}_{\mathrm{Lc},s,t}, P^{\mathrm{E}}_{\mathrm{Lc},s,t}, \rho_{s,t}) = {} & F_{\mathrm{MTA-TSTD}}(P^{\mathrm{T}}_{\mathrm{Lc},s,t}) + F_{\mathrm{MOPF-TSPD}}(P^{\mathrm{E}}_{\mathrm{Lc},s,t}) \\ & + \sum_{t\in\Omega_{\mathrm{T}}}\sum_{s\in\Omega_{\mathrm{WCS}}} \rho_{s,t}(P^{\mathrm{T}}_{\mathrm{Lc},s,t} - P^{\mathrm{E}}_{\mathrm{Lc},s,t}) + \sum_{t\in\Omega_{\mathrm{T}}}\sum_{s\in\Omega_{\mathrm{WCS}}} \frac{b}{2}\left\| P^{\mathrm{T}}_{\mathrm{Lc},s,t} - P^{\mathrm{E}}_{\mathrm{Lc},s,t}\right\|_2^2 \end{aligned} \tag{76}$$

This augmented Lagrangian function can be decomposed into three subproblems: $P^{\mathrm{T}}_{\mathrm{Lc},s,t} - update$ subproblem 1, $P^{\mathrm{E}}_{\mathrm{Lc},s,t} - update$ subproblem 2, and Lagrange multipliers updating. Specifically, the MTA-TSTD corresponds to $P^{\mathrm{T}}_{\mathrm{Lc},s,t} - update$ subproblem 1, and the MOPF-TSPD corresponds to $P^{\mathrm{E}}_{\mathrm{Lc},s,t} - update$ subproblem 2. The detailed model is provided below:

$$P^{\mathrm{T},k+1}_{\mathrm{Lc},s,t} \in \underset{P^{\mathrm{T}}_{\mathrm{Lc},s,t}\in\Omega_{\mathrm{MTA-TSTD}}}{\operatorname{argmin}} \left\{ F_{\mathrm{MTA-TSTD}} + \sum_{t\in\Omega_{\mathrm{T}}}\sum_{s\in\Omega_{\mathrm{WCS}}} \rho_{s,t}(P^{\mathrm{T}}_{\mathrm{Lc},s,t} - P^{\mathrm{E},k}_{\mathrm{Lc},s,t}) + \sum_{t\in\Omega_{\mathrm{T}}}\sum_{s\in\Omega_{\mathrm{WCS}}} \frac{b}{2}\left\| P^{\mathrm{T}}_{\mathrm{Lc},s,t} - P^{\mathrm{E},k}_{\mathrm{Lc},s,t}\right\|_2^2 \right\} \tag{77}$$

$$P^{\mathrm{E},k+1}_{\mathrm{Lc},s,t} \in \underset{P^{\mathrm{E}}_{\mathrm{Lc},s,t}\in\Omega_{\mathrm{OPF-DR}}}{\operatorname{argmin}} \left\{ F_{\mathrm{MOPF-TSPD}} + \sum_{t\in\Omega_{\mathrm{T}}}\sum_{s\in\Omega_{\mathrm{WCS}}} \rho_{s,t}(P^{\mathrm{T},k+1}_{\mathrm{Lc},s,t} - P^{\mathrm{E}}_{\mathrm{Lc},s,t}) + \sum_{t\in\Omega_{\mathrm{T}}}\sum_{s\in\Omega_{\mathrm{WCS}}} \frac{b}{2}\left\| P^{\mathrm{T},k+1}_{\mathrm{Lc},s,t} - P^{\mathrm{E}}_{\mathrm{Lc},s,t}\right\|_2^2 \right\} \tag{78}$$

$$\rho^{k+1}_{s,t} = \rho^{k}_{s,t} + b\left(P^{\mathrm{T},k+1}_{\mathrm{Lc},s,t} - P^{\mathrm{E},k+1}_{\mathrm{Lc},s,t}\right), \quad \forall s\in\Omega_{\mathrm{WCS}}, t\in\Omega_{\mathrm{T}} \tag{79}$$

where $\Omega_{\mathrm{MTA-TSTD}}$ and $\Omega_{\mathrm{MOPF-TSPD}}$ represent the constraint sets of MTA-TSTD and MOPF-TSPD models, respectively.

3. Solution Methodology

3.1. Adaptive Effective Path Generation Algorithm for Solving MTA-TSTD Model

The adaptive effective path generation algorithm is designed to solve the MTA-TSTD model, which iteratively recognizes a subset of paths that are most likely taken. The detailed algorithm process is outlined in Algorithm 1.

Remark 3. *The adaptive effective path generation algorithm can be regarded as the process of optimal route, departure times, and charging plan for individual EV and GV drivers. To support this, an online traveling and charging navigation platform should be designed. This platform would allow drivers to input their origin, destination, departure time, and SoC level, enabling them to receive optimal traveling and charging guidance, Concurrently, the TSO would collect traffic demands data of OD pairs and implement the price-based management accordingly.*

Algorithm 1: Adaptive effective path generation algorithm.

1. Initialize Traffic Flow Pattern: Let $\psi_a^t = 0, \quad \forall a \in \Omega_A, t \in \Omega_T$, solve EPGM-EVs and EPGM-GVs for each OD pair $w \in \Omega_{OD,t}$ in each period $t \in \Omega_T$, and then build initial effective path sets Ω_{KEV} and Ω_{KGV}.
2. Solve MTA-TSTD Model: Using the current effective path sets Ω_{KEV} and Ω_{KGV}, solve the MTA-TSTD model, determine the traffic flow $\psi_a^{t,*}, \quad \forall a \in \Omega_A, t \in \Omega_T$ on each road in each period $t \in \Omega_T$. And then update travelling costs $\zeta_{EV,ke,w}^t$ and $\zeta_{GV,kg,w}^t$ for each path, find minimal travelling expenses $\mu_{EV,w}^t$ and $\mu_{GV,w}^t$ for each OD pair $w \in \Omega_{OD}$ in each period $t \in \Omega_T$.
3. Solve EPGM-EVs and EPGM-GVs: With the obtained traffic flow $\psi_a^{t,*}, \quad \forall a \in \Omega_A, t \in \Omega_T$, solve EPGM-EVs and EPGM-GVs for each OD pair $w \in \Omega_{OD,t}$ in each period $t \in \Omega_T$, the optimal solutions are new effective paths v_{ke}^t and v_{kg}^t, and corresponding travelling costs are $\kappa_{EV,ke,w}^t$ and $\kappa_{GV,kg,w}^t$.
4. Convergence Check: If $\kappa_{EV,ke,w}^t \geq \mu_{EV,w}^t, \kappa_{GV,kg,w}^t \geq \mu_{GV,w}^t, \forall w \in \Omega_{OD,t}, t \in \Omega_T$, terminate the procedure and report the current traffic flow on each road; otherwise, if $\kappa_{EV,ke,w}^t < \mu_{EV,w}^t$ for some OD pairs, $\Omega_{KEV,w}^t \leftarrow [\Omega_{KEV,w}^t, v_{ke}^t]$; if $\kappa_{GV,kg,w}^t < \mu_{GV,w}^t$ for some OD pairs, $\Omega_{KGV,w}^t \leftarrow [\Omega_{KGV,w}^t, v_{kg}^t]$; Update effective path sets Ω_{KEV} and Ω_{KGV}, and go to step 2.

3.2. ETN–PDN Interaction Algorithm for Solving Distributed Coordinated Operation Model

The distributed coordinated operation model for CTPES can be iteratively solved by addressing the $P_{Lc,s,t}^T - update$ subproblem 1 and $P_{Lc,s,t}^E - update$ subproblem 2, as well as updating Lagrange multipliers. The iteration process will terminate when the primal and dual residuals satisfy the convergence criteria defined in Equations (80) and (81). The ETN–PDN interaction process is detailed in Algorithm 2.

$$\max\left\{\left|P_{Lc,s,t}^{T,k+1} - P_{Lc,s,t}^{E,k+1}\right| \forall s \in \Omega_{WCS}, t \in \Omega_T\right\} \leq \varepsilon^{pri} \tag{80}$$

$$\max\left\{\left|P_{Lc,s,t}^{T,k+1} - P_{Lc,s,t}^{T,k}\right|, \left|P_{Lc,s,t}^{E,k+1} - P_{Lc,s,t}^{E,k}\right| \forall s \in \Omega_{WCS}, t \in \Omega_T\right\} \leq \varepsilon^{dual} \tag{81}$$

Algorithm 2: ETN–PDN interaction algorithm.

1. Initialize: Set the current iteration count $k = 0$, and initialize the charging load $P_{Lc,s,t}^{E,k} = 0, \forall s \in \Omega_{WCS}, t \in \Omega_T$ in $P_{Lc,s,t}^E - update$ subproblem 2, nodal marginal electricity prices $\lambda_a^{t,k} = 0, \forall a \in \Omega_A, t \in \Omega_T$, and Lagrange multipliers $\rho_{s,t}^k = 0, \forall s \in \Omega_{WCS}, t \in \Omega_T$.
2. Solve subproblem 1: Utilize Algorithm 1 to solve $P_{Lc,s,t}^T - update$ subproblem 1, obtain charging load $P_{Lc,s,t}^{T,*}, \forall s \in \Omega_{WCS}, t \in \Omega_T$ in ETN. Then set $P_{Lc,s,t}^{T,k+1} = P_{Lc,s,t}^{T,*}$.
3. Solve subproblem 2: Solve $P_{Lc,s,t}^E - update$ subproblem 2 to determine nodal marginal electricity prices $\lambda_a^{t,*} = 0, \forall a \in \Omega_A, t \in \Omega_T$, and charging load $P_{Lc,s,t}^{E,*}, \forall s \in \Omega_{WCS}, t \in \Omega_T$ in PDN. Set $\lambda_a^{t,k+1} = \lambda_a^{t,*}, P_{Lc,s,t}^{E,k+1} = P_{Lc,s,t}^{E,*}$.
4. Update Lagrange multipliers: Update Lagrange multipliers $\rho_{s,t}^{k+1}, \forall s \in \Omega_{WCS}, t \in \Omega_T$ based on the charging load $P_{Lc,s,t}^{T,k+1}$ and $P_{Lc,s,t}^{E,k+1}$.
5. Check Convergence: If the convergence criteria specified in Equations (80) and (81) are satisfied, terminate the iteration process. Otherwise, return to Step 2.

The overall flowchart of the solution methodology (Algorithms 1 and 2) is summarized in Figure 2.

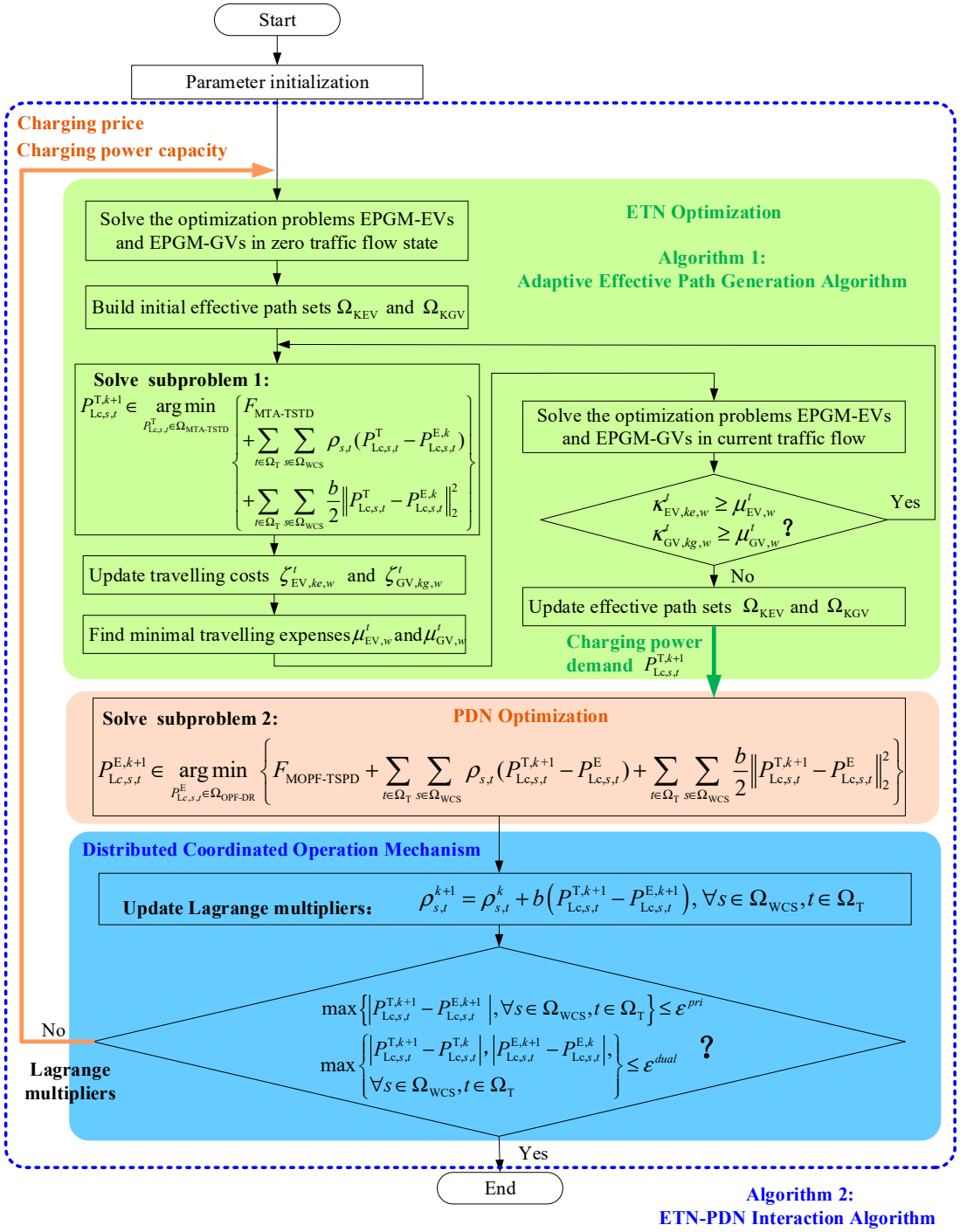

Figure 2. The overall flowchart of the solution methodology.

4. Case Studies

In this section, two test systems are adopted to evaluate the effectiveness of the proposed models and algorithms.

4.1. Test System 1

The test system 1 is a simple CPTES comprising a 3-node ETN and a 5-node PDN. The topological structure is depicted in Figure 3 [11]. The ETN features a single OD pair (from T1 to T3), three nodes, and five roads/links. All roads are equipped with DWC facilities, each powered by a corresponding bus in the PDN. The PDN consists of five buses, five

distribution lines, and a local generator connected to bus 2. The infrastructure parameters of the ETN and its coupling relationship with the PDN are detailed in Table 1.

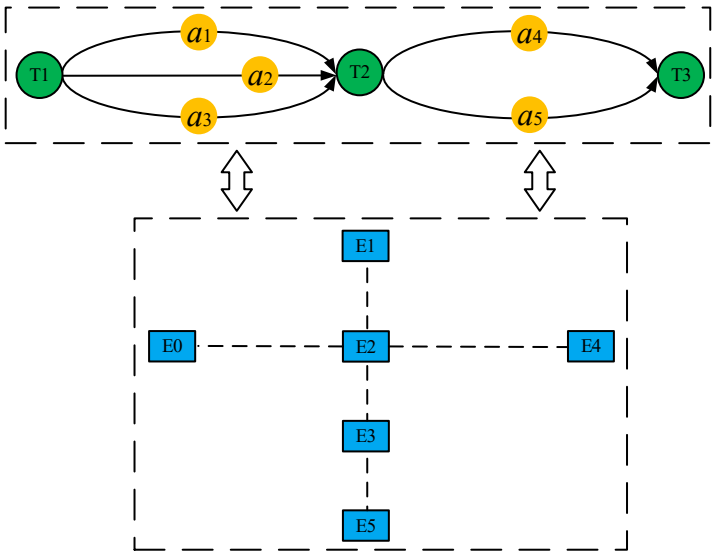

Figure 3. Topology of test system 1.

Table 1. Parameters of the ETN infrastructure in test system 1.

Road	Flow Capacity of Road C_a (p.u.)	Maximum Charging Energy L_a (kWh)	Road Distance d_a (km)	Free Flow Travel Time χ_a^0 (min)	Connected PDN Bus
a_1	6	3	8.00	6	E2
a_2	8	5	13.33	10	E4
a_3	5	3.25	8.67	6.5	E5
a_4	9.8	2.5	6.67	5	E3
a_5	7	2.75	7.33	5.5	E1

We simulate the afternoon commuting hours (16:00–20:00), a period often characterized by congestion. The initial curves of traffic demand and regular power demand are shown in Figure 4. The peak traffic demand occurred at 18:00, while the peak regular power load occurred at 20:00. Among the traffic demand, 40% consisted of EVs requiring charging. Each EV has a battery capacity of 24 kWh, with an energy consumption rate of 0.18 kWh/km. The base values of traffic flow and power load are set at 100 veh/h and 10 MVA, respectively. In the MTA-TSTD model, the elasticity coefficient matrix E is sourced from the literature [20]. In the MOPF-TSPD, the initial electricity price for regular power loads during peak periods is set as USD 1800/p.u., with acceptable price adjustment limits set at 0.8 and 1.2 times the initial electricity price. The upward and downward spinning reserve requirements are set at 10% of the total load for each period. The local generator has a generation capacity of 0.6 p.u, and a ramp rate of 0.5 times its capacity. The lower and upper voltage boundaries are $\sqrt{U_j^{\min}} = 0.9110$ and $\sqrt{U_j^{\max}} = 1.05$. In addition, we adopt the following parameter settings: $e_{tt} = -0.6$, $e_{t\tau} = 0.15$, $a_g = 200$ USD/p.u., $b_g = 1300$ USD/p.u., and $\rho_{\text{sub}}^t = 1500$ USD/p.u.

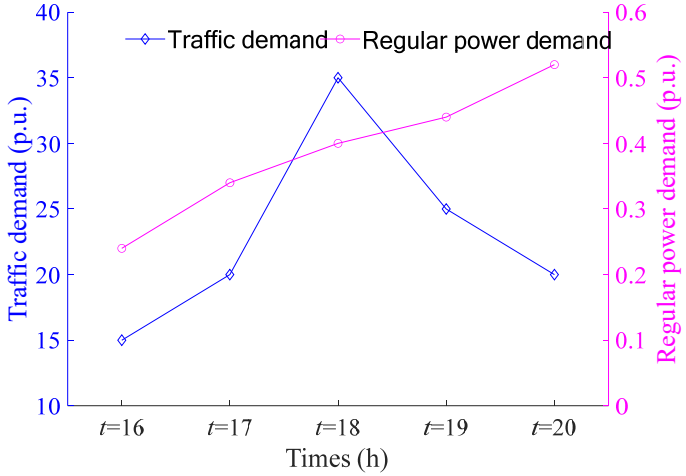

Figure 4. Initial curves of traffic demand and regular power demand from 16:00 to 20:00 in test system 1.

In order to analyze in detail the impact of time-shiftable traffic demand on CPTES and demonstrate the effectiveness of the proposed models and algorithms, we consider the following five cases:

Case 1: Independent operation between ETN and PDN without considering time-shiftable traffic demand.

Case 2: Independent operation between ETN and PDN with time-shiftable traffic demand.

Case 3: Coordinated operation between ETN and PDN without considering time-shiftable traffic and regular power demand.

Case 4: Coordinated operation between ETN and PDN, considering time-shiftable traffic demand based on Case 3.

Case 5: Coordinated operation between ETN and PDN, considering both time-shiftable traffic and regular power demand based on Case 4.

In Case 1 and Case 3, nonshiftable traffic demand is distributed according to single-period UE, in which travelers do not switch departure time but merely determine route choice. In Case 1 and Case 2, the ETN and PDN operate independently, with no interaction between the two networks. In this situation, the nodal marginal price (charging price) does not influence the departure time, route choice, or charging decisions of EV drivers. In other words, drivers choose the shortest travel time routes based on their preferences and will charge as much as possible during the journey until their batteries are fully charged. Additionally, the flexibility of regular power demand in PDN is not considered.

To ensure a feasible solution for Case 1 and 2 under high traffic density, it is assumed that the lower bound of voltage can be violated at the cost of an additional high penalty. Consequently, the total operation cost of PDN $F_{\mathrm{MOPF-TSPD}}$ in the MOPF-TSPD is adjusted as follows:

$$\begin{aligned} F_{\mathrm{MOPF-TSPD}} &= F_{\mathrm{sub}} + F_{\mathrm{G}} + F_{\mathrm{peak-Valley}} + F_{\mathrm{U-penalty}} \\ &= \rho_{\mathrm{sub}} \sum_{t\in\Omega_{\mathrm{T}}} \sum_{j\in\Omega_{\mathrm{sub}}} P^{t}_{\mathrm{sub},j} + \sum_{t\in\Omega_{\mathrm{T}}} \sum_{g\in\Omega_{\mathrm{G}}} \left[a_g (P^{t}_{\mathrm{G},g})^2 + b_g P^{t}_{\mathrm{G},g} \right] \\ &+ \rho_{\mathrm{peak-Valley}} \left[P^{\max}_{\mathrm{L}} - P^{\min}_{\mathrm{L}} \right] + \kappa \sum_{t\in\Omega_{\mathrm{T}}} \sum_{j\in\Omega_{\mathrm{N}}} \Delta U^{t}_{j} \end{aligned} \tag{82}$$

Here, the penalty coefficient is chosen as $\kappa = 50000$ USD/p.u. [26]; meanwhile, the voltage boundary constraints in (64) are adjusted to the following:

$$U^{\min}_{j} - \Delta U^{t}_{j} \le U^{t}_{j} \le U^{\max}_{j},\ \Delta U^{t}_{j} \ge 0,\ \ \forall j \in \Omega_{\mathrm{N}}, t \in \Omega_{\mathrm{T}} \tag{83}$$

4.1.1. Impact of Time-Shiftable Traffic Demand on ETN and PDN

This subsection analyzes the impact of time-shiftable traffic demand on ETN and PDN using Cases 1 and 2, and then demonstrates the necessity for coordinated management in the coupled networks.

1. Impact of time-shiftable traffic demand on ETN

Figures 5 and 6 show the variations in traffic demand and traffic flow distribution during the evening peak period for Case 1 and Case 2. From Figures 5 and 6a, it can be observed that in Case 1, the majority of traffic users are concentrated around 18:00 as their initial plan, resulting in severe congestion compared to other times. In contrast, traffic demand at 16:00 is minimal, and the ETN operates more smoothly. During this period, most traffic users prefer road with shorter travel time. For example, between traffic nodes T1 and T2, shorter roads a_1 and a_3 are allocated traffic flow, while the traffic flow in the longer road is zero (as shown by the absence of traffic flow on road a_2 at 16:00 in Figure 6a). This comparison highlights the underutilization of roads at 16:00 and indicates the potential for peak-shaving and valley-filling in the ETN.

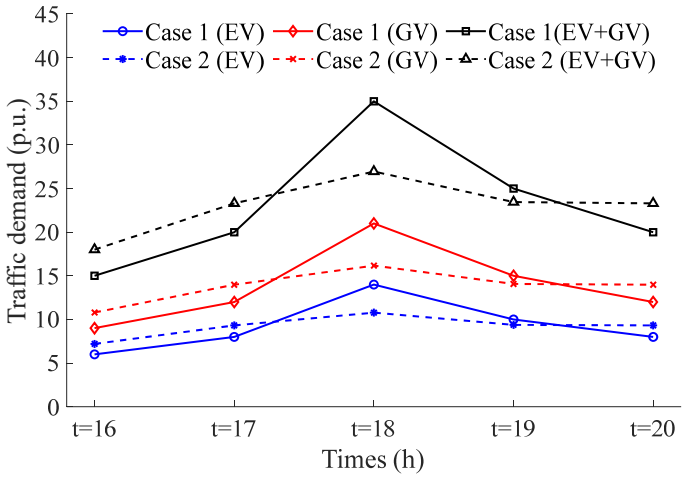

Figure 5. Traffic demand profiles from 16:00 to 20:00 in Cases 1–2.

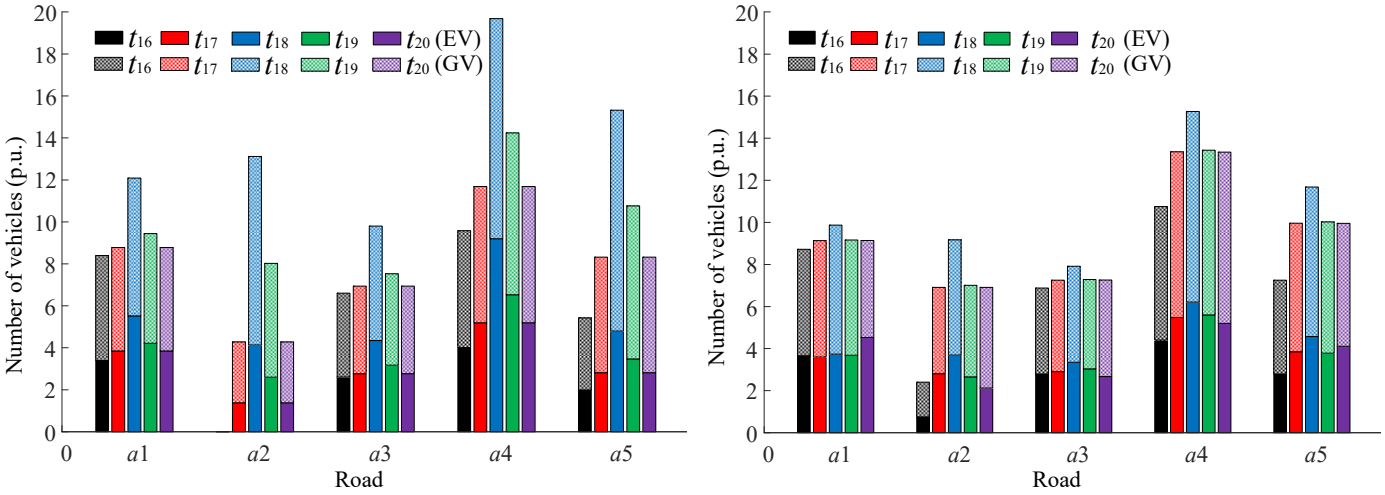

Figure 6. Traffic flow distribution of the ETN from 16:00 to 20:00: (**a**) in Case 1, (**b**) in Case 2.

In Case 2, the flexibility of traffic demand is leveraged by considering the interaction between user departure times and road congestion. This approach fully explores the complementary advantages of different time periods within the evening peak hours. Figures 5 and 6b

show that traffic demand during the peak period (18:00–19:00) is significantly reduced, while traffic demand in other periods is moderately increased. This results in a more uniform distribution of traffic flow from 16:00 to 20:00, indicating a more efficient utilization of ETN.

2. Impact of time-shiftable traffic demand on PDN

Figures 7 and 8 illustrate the variations in charging load and node voltage in the PDN during the evening peak period for both Case 1 and Case 2. It can be observed that in Case 1, where traffic demand is nonshiftable, the peak charging load occurs at 18:00, which causes a significant drop in voltages at buses E3 and E5, falling well below safe operational limits. In contrast, Case 2 leverages the flexibility of time-shiftable traffic demand. As a result, the peak charging load decreases from 0.88 p.u. to 0.68 p.u., representing a reduction of nearly 25%. Additionally, the charging load at 17:00 is reduced, while there is a slight increase in other periods. This adjustment reduces the peak-to-valley difference in charging load between 16:00 and 20:00, leading to a more uniform load distribution. Consequently, the voltage levels and overall operational performance of the PDN are significantly improved.

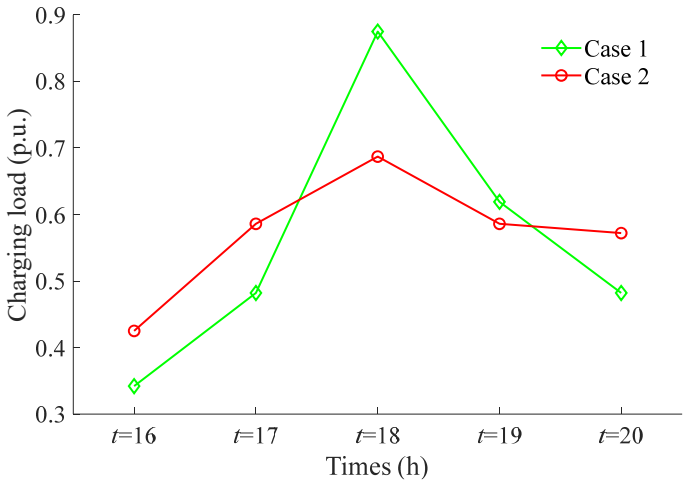

Figure 7. Charging load profiles from 16:00 to 20:00 in Cases 1–2.

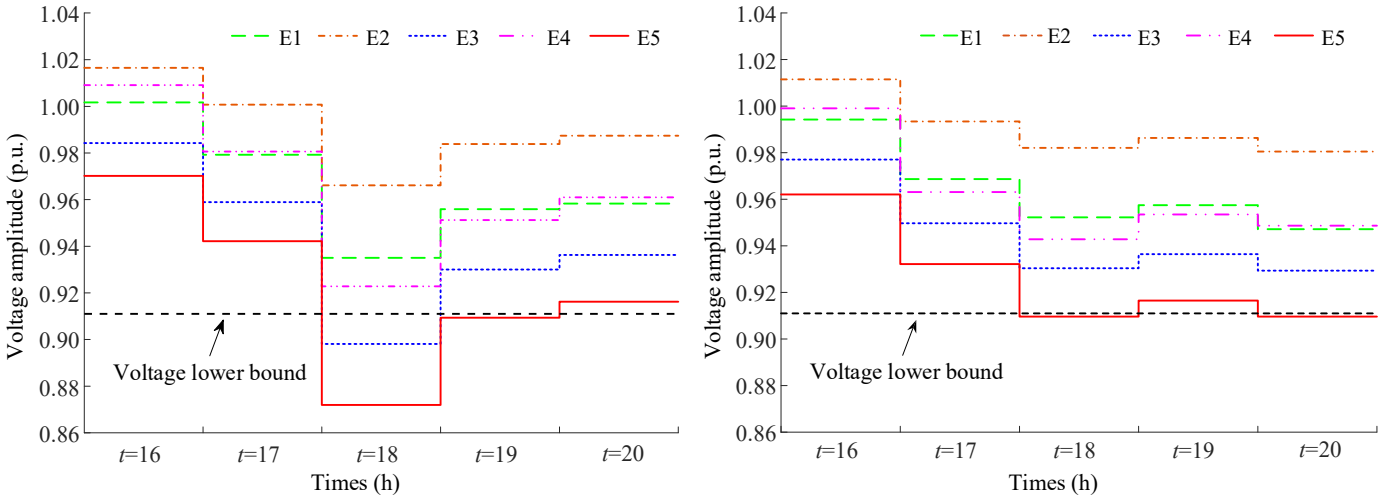

Figure 8. Node voltage level of PDN from 16:00 to 20:00: (**a**) in Case 1, (**b**) in Case 2.

However, it is worth noting that time-shiftable traffic demand also increases the charging load at 20:00, as shown by the charging load curve in Case 2 (Figure 7). This exacerbates the already high load levels during the regular power demand peak, leading

to a voltage violation at the E5 bus at 20:00, as depicted in Figure 8b. Therefore, while time-shiftable traffic demand in the independent operation mode effectively smooths out the total traffic demand and charging load curves, alleviating peak-hour traffic congestion and improving voltage levels, voltage violation still exists in both networks. This indicates the necessity for appropriate coordinated management methods for CPTES to ensure safe and economical operation throughout the peak period, which is discussed in Section 4.1.3.

4.1.2. Effectiveness of Effective Path Generation Models with EV Battery SOC

To demonstrate the effectiveness of the proposed effective path generation models with EV battery SOC, this subsection compares them with traditional path generation models that do not consider EV battery SOC. Specifically, based on Case 5, we designed Case 6 by removing the relevant SOC constraints for comparative analysis. In Case 6 (traditional path generation models without EV battery SOC), charging energy $E^t_{a,ke,w}$ is not optimized; instead, a constant charging energy is assumed, which is set to maximum charging energy L_a. In our proposed model (Case 5), the parameters are defined as follows: the minimum threshold m for the SOC for EVs is set at 10% of the battery capacity, the initial SOC of EVs is uniformly set to 30% of the battery capacity, and by the end of the trip, the SOC must be maintained at or above 30% of the battery capacity.

Table 2 presents the operational cost results for ETN and PDN objective functions in Cases 5 and 6. It is evident that in Case 6, the total charging cost, purchasing electricity and generation costs are higher than those in Case 5, while also exhibiting a larger peak-to-valley load difference. This is because, in traditional methods, the charging energy for EVs is fixed and cannot be regulated or optimized. Drivers attempt to fill their EV batteries based on the maximum charging capacity provided by DWC roads, resulting in relatively high charging loads. This, in turn, increases the PDN purchasing electricity and generation costs, leading to higher charging prices and an increase in total charging costs of ETN. These results indicate that our method contributes to better power load balancing by optimizing charging energy $E^t_{a,ke,w}$ with consideration of EV battery SOC.

Table 2. Operational costs of objective function in Cases 5–6.

Cases	Total Operational Costs for ETN		Total Operational Costs for PDN		
	Total Delay Cost F_{DT} (USD)	Total Charging Cost F_{CH} (USD)	Purchasing Electricity and Generation Cost F_{sub}+F_G (USD)	Penalty Cost for Load Peak-Valley Differences $F_{peak\text{-}Valley}$ (USD)	Penalty Cost for Voltage Violations (USD)
5	26,417.99	2750.17	5289.51	465.84	0.00
6	26,419.84	4183.68	6601.59	559.32	0.00

As an example from Case 5 at 18:00, Figure 9 presents SOC of EVs at each road node and charging energy $E^t_{a,ke,w}$ at DWC road along the effective travel path. It is can be seen that the proposed EPGM-EVs identifies two effective paths from origin T1 to destination T3: path $a_1 - a_4$ and path $a_3 - a_5$ and path, with distributed traffic flows of 998 and 80 vehicles, respectively. Additionally, the charging energy $E^t_{a,ke,w}$ of EVs at each DWC road along the travel route is optimized, and all the EVs battery SOC constraints in EPGM-EVs are met, ensuring that their batteries do not run out and avoiding range anxiety of EV drivers due to battery technology limitations. These results further demonstrate that the proposed EPGM-EVs effectively captures the SOC of EVs across different travel paths, while also optimizing and regulating EV charging energy along the travel routes.

Therefore, the proposed effective path generation models with EV battery SOC have significant advantages compared to traditional methods, which often ignore battery status and focus solely on distance or time. This model not only provides more realistic and reliable routes for EVs, but also promotes the coordinated operation of the PDN and ETN by optimizing charging energy with consideration of EV battery SOC.

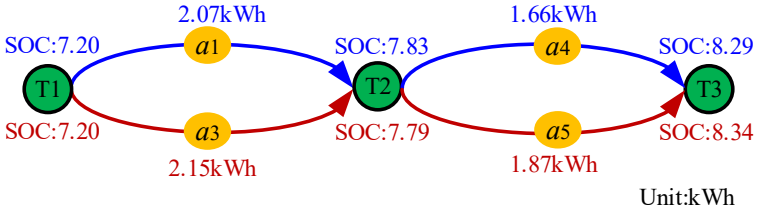

Figure 9. SOC of EVs at each road node and charging energy for EVs at DWC road along the effective travel path.

4.1.3. Effectiveness of the Proposed Distributed Coordinated Operation Model Considering IDRs in Congestion Alleviation and Cost Reduction

This subsection evaluates the effectiveness of the proposed distributed coordinated operation model considering IDRs for decreasing congestion levels and reducing total operating cost in the ETN and PDN by analyzing Cases 3–5.

1. The operational cost results for ETN and PDN objective functions

The operational cost results for ETN and PDN objective functions in Cases 3–5 are presented in Table 3. It is evident that in Cases 3–5, the penalty costs for voltage violations in PDN are all zero, indicating that the voltage safety constraints are met in all scenarios. Compared to Cases 1–2, the coordinated operation management for CPTES enables EV users to respond to charging electricity prices during the evening peak period, thereby adjusting their route choices and charging roads. This approach significantly improves and enhances the operational performance of the PDN, particularly alleviating voltage violations caused by congestion in the PDN.

Table 3. Operational costs of objective function in Cases 3–5.

Cases	Total Operational Costs for ETN		Total Operational Costs for PDN		
	Total Delay Cost F_{DT} (USD)	Total Charging Cost F_{CH} (USD)	Purchasing Electricity and Generation Cost F_{sub}+F_G (USD)	Penalty Cost for Load Peak-Valley Differences $F_{peak\text{-}Valley}$ (USD)	Penalty Cost for Voltage Violations (USD)
3	28,091.28	2770.51	5380.15	899.81	0.00
4	26,417.89	2753.75	5371.67	697.07	0.00
5	26,417.99	2750.17	5289.51	465.84	0.00

However, in Case 3, the total operational costs for both ETN (including total delay and charging costs) and PDN are higher compared to Case 4 and Case 5, with particularly significant differences observed in total delay costs and penalty costs for load peak-to-valley differences. Because Case 4 leverages the flexibility of time-shiftable traffic demand to redistribute the peak period (18:00–19:00) traffic demand to other off-peak periods, it results in a more uniform traffic flow distribution from 16:00 to 20:00 and a smoother charging load curve. Consequently, Case 4 incurs lower total delay costs and peak-to-valley penalty costs compared to Case 3. Building on Case 4, Case 5 further incorporates demand response for regular power loads and adjusts the consumption behavior of flexible noncharging loads under "peak shaving and valley filling" state of the ETN, thereby achieving a greater smoothing effect on the PDN's load curve during peak periods. As a result, Case 5 has the lowest penalty costs for load peak-to-valley differences.

In summary, Case 5 has the lowest operational costs in both the ETN and PDN. Compared to Case 3, it reduces total operational costs for the ETN by USD 1693.63, representing a 5.48% decrease, and for the PDN by USD 524.61, representing an 8.35% decrease. Therefore, the proposed distributed coordinated operation model effectively reduces the total operating costs for both the ETN and PDN by considering time-shiftable traffic and power demand, along with the implementation of IDRs.

2. Effect of flexible traffic and power demand on congestion management

To further demonstrate the effect of flexible traffic and power demand on congestion management, Figures 10 and 11 present the variation curves of total traffic demand in ETN

and total power load in PDN from 16:00 to 20:00. Table 4 outlines the effective path, travel time, travel cost, and path traffic flow at 18:00 for Cases 3 and 5. Additionally, Table 5 provides details on the corresponding peak and valley loads in PDN, along with their occurrence times.

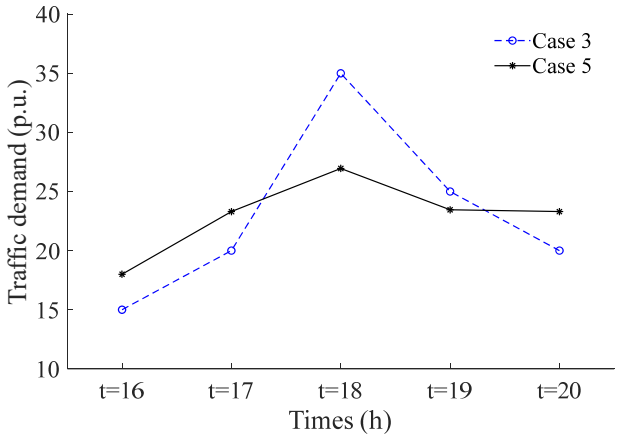

Figure 10. Total traffic demand variation curves in ETN from 16:00 to 20:00 in Cases 3 and 5.

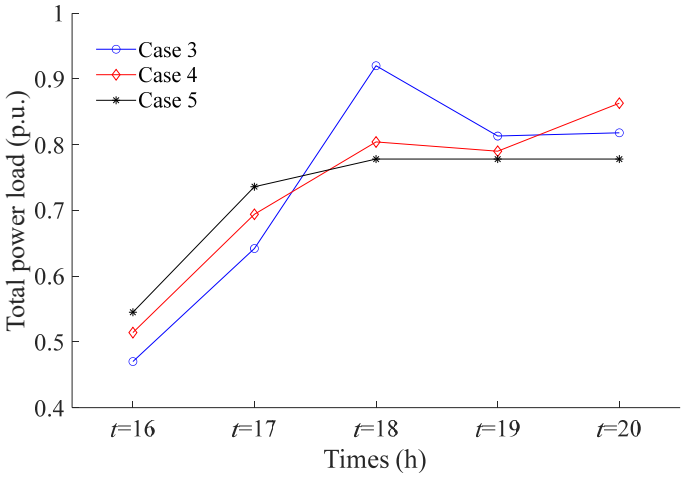

Figure 11. Total power load profiles from 16:00 to 20:00 in Cases 3–5.

Table 4. Effective path, travel time, travel cost, and path traffic flow (18:00 in Cases 3 and 5).

Effective Path		Case 3			Case 5		
		Travel Time (min)	Travel Cost (USD)	Traffic Flow (veh)	Travel Time (min)	Travel Cost (USD)	Traffic Flow (veh)
GV-Path	$a_3 - a_5$	37.91	6.32	792	21.93	3.66	708
	$a_2 - a_4$	37.91	6.32	753	21.93	3.66	530
	$a_2 - a_5$	37.91	6.32	555	21.93	3.66	380
EV-Path	$a_1 - a_4$	38.31	6.99	1215	22.32	4.32	998
	$a_3 - a_5$	37.91	6.99	185	21.93	4.32	80

Table 5. Peak values and valley values of total power load in Cases 3–5.

Cases	Peak Times (h)	Peak Value (MW)			Valley Times (h)	Valley Value (MW)		
		Regular Power Load	Charging Load	Total Power Load		Regular Power Load	Charging Load	Total Power Load
3	18:00	4.00	5.20	9.20	16:00	2.40	2.30	4.70
4	20:00	5.20	3.43	8.63	16:00	2.40	2.74	5.14
5	18:00~20:00	3.74/4.28/4.32	4.04/3.50/3.46	7.78	16:00	2.71	2.74	5.45

From Figure 10, it is clear that, compared to Case 3, Case 5 shows a smoother load curve during the evening peak period (16:00–20:00). Notably, as shown in Table 4, during the traffic peak at 18:00, both GVs and EVs experience significant reductions in travel time and costs on their effective travel paths. This improvement contributes to the total traffic delay cost decreasing from USD 28,091.28 in Case 3 to USD 26,417.99 in Case 5. These results indicate that the proposed model is effective in alleviating traffic congestion.

As indicated in Figure 11, the total power load curve in Case 3 exhibits a larger peak-to-valley difference due to the limitation that travelers do not switch departure time but merely determine route choice and charging energy. The peak and valley occur at 18:00 and 16:00 in Case 3, respectively. In contrast, Case 4 smooths the total load curve by considering the flexibility of time-shiftable traffic demand, allowing EV travelers to either advance or delay their departure times. The peak and valley occur at 20:00 and 16:00 in Case 4, respectively. In Case 5, which considers the flexibility of both time-shiftable traffic and regular power demand simultaneously, the peak-to-valley difference for both charging and regular loads is further reduced, resulting in a flattened total load curve from 18:00 to 20:00. Therefore, the flexibility of time-shiftable traffic and power demand has a positive effect on congestion management for PDN.

However, from Figure 11 and Table 5, it can be observed that the peak value of total power load in PDN shifts to 20:00 in Case 4, which coincides with the peak period for regular power consumption. At 20:00, the total power load in Case 4 is higher than in Case 3 and Case 5. This occurs because, after considering the flexibility of time-shiftable traffic demand, the charging demand during the peak periods of 18:00 and 19:00 is redistributed to off-peak periods, leading to an increase in the charging load of PDN at 20:00. This exacerbates the already high load level during the regular load peak period, causing the total power load in Case 4 at 20:00 to surpass that in Case 3. In contrast, Case 5 coordinates the demand response of regular power load, effectively shifting the regular power demand at 20:00, thereby avoiding the creation of another load peak due to the time-shiftable traffic demand.

Figure 12 presents the electricity prices for regular power demand and load values before and after demand response from 16:00 to 20:00 in Case 5. This indicates that Case 5, building on Case 4, further adjusts the consumption behavior of flexible regular power demand by coordinating the flexibility of time-shiftable traffic demand. By implementing real-time electricity prices for regular power demand, Case 5 effectively shifts the regular power load during peak period to off-peak periods, achieving true temporal and spatial coordination between the ETN and PDN.

Figure 13 presents the node marginal charging electricity price variations for different charging road from 16:00 to 20:00 in Cases 3–5. It is evident that in Case 3, there is a significant difference in node marginal charging electricity prices across different time periods, with the charging price being notably high during the traffic demand peak at 18:00. In contrast, Cases 4 and 5 show a more gradual change in node marginal charging electricity prices throughout the time periods. Particularly in Case 5, the node marginal charging electricity prices are more stable across time periods, demonstrating the significant advantages of considering both time-shiftable traffic demand and regular load demand, as well as IDRs. This promotes the safe, economical, and coordinated operation of the PDN and ETN during the evening peak hours.

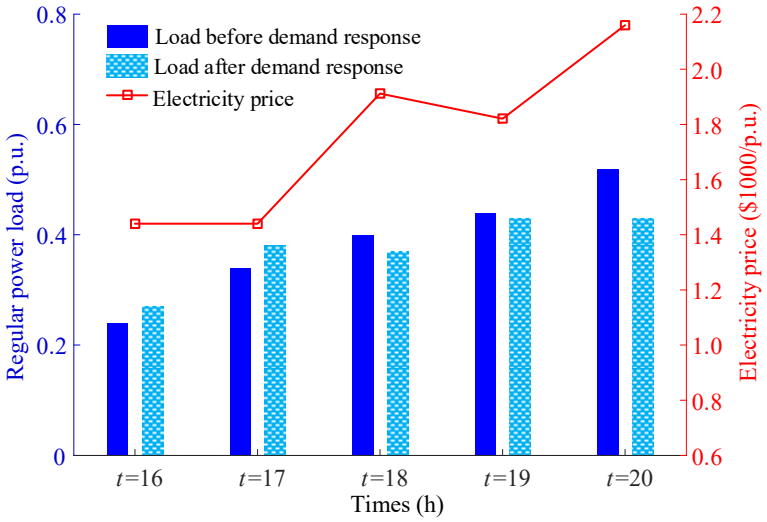

Figure 12. Electricity price profile for regular power demand and load value before and after demand response from 16:00 to 20:00 in Case 5.

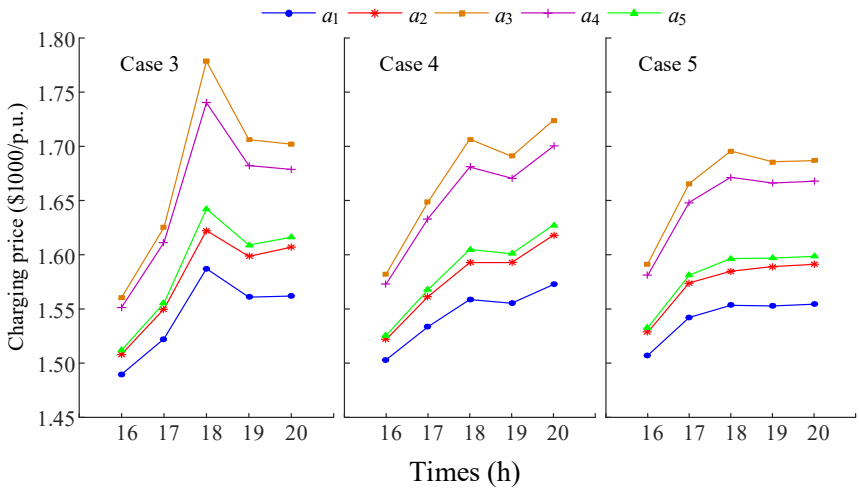

Figure 13. Charging price profiles of each road from 16:00 to 20:00 in Cases 3–5.

4.2. Test System 2

Test system 2 is a larger-scale CPTES composed of a 12-node ETN and a 20-node PDN. The topological structure is depicted in Figure 14 [26]. The ETN features a typical inner and outer ring structure and includes 11 OD pairs and 20 traffic nodes, with road parameters set as shown in Table 6. Similar to test system 1, the PDN is coupled with the ETN through DWC roads, which comprises 20 buses and 20 distribution lines. Additionally, the PDN has four local generators with identical parameters at nodes E7, E10, E11, and E14, each with a capacity of 1.8 p.u., and cost coefficients specified as $a_g = 200$ USD/p.u. and $b_g = 1300$ USD/p.u. The impedance parameters for the distribution lines are provided in [26]. During the evening peak period (16:00–20:00), the initial load curves for traffic demand and regular power demand are shown in Figure 15, with peak values of 90 p.u. and 2.08 p.u., respectively. The MTA-TSTD, MOPF-TSPD, and other parameter settings are the same as those in test system 1 and are not repeated here.

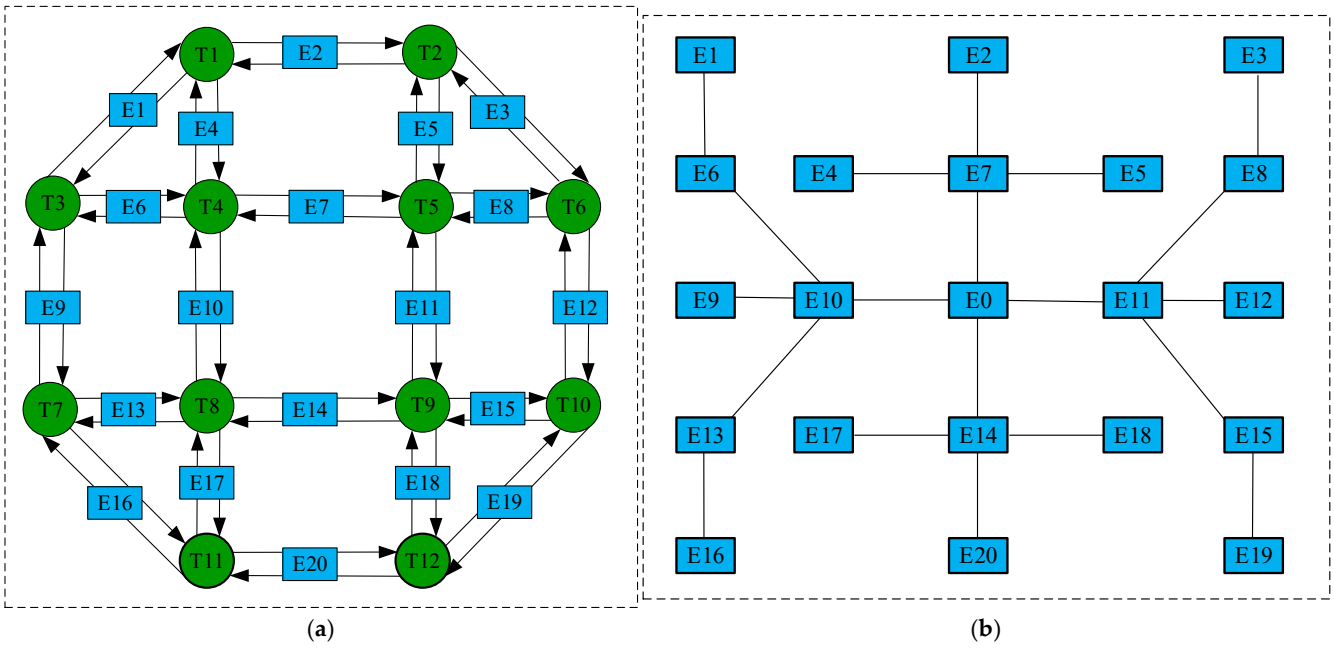

Figure 14. Topology of test system 2: (**a**) ETN, (**b**) PDN.

Table 6. Parameters of the ETN infrastructure in test system 2.

Road	Flow Capacity of Road C_a (p.u.)	Road Distance d_a (km)	Free Flow Travel Time χ_a^0 (min)	Road	Flow Capacity of Road C_a (p.u.)	Road Distance d_a (km)	Free Flow Travel Time χ_a^0 (min)
T1–T3	10.80	6.0	8.00	T5–T9	8.28	12.5	16.67
T1–T2	12.00	10	13.33	T6–T10	12.00	10.5	14.00
T2–T6	10.20	6.5	8.67	T7–T8	5.34	5.8	7.73
T1–T4	5.88	5.0	6.67	T8–T9	7.92	11	14.67
T2–T5	4.74	5.5	7.33	T9–T10	5.49	5.9	7.87
T3–T4	5.10	6.0	8.00	T7–T11	10.50	6.3	8.40
T4–T5	8.10	12	16.00	T8–T11	5.86	5.7	7.60
T5–T6	4.92	6.5	8.67	T9–T12	5.38	5.8	7.73
T3–T7	11.40	10.2	13.60	T12–T10	10.92	6.1	8.13
T4–T8	8.40	11.5	15.33	T11–T12	12.00	9.8	13.07

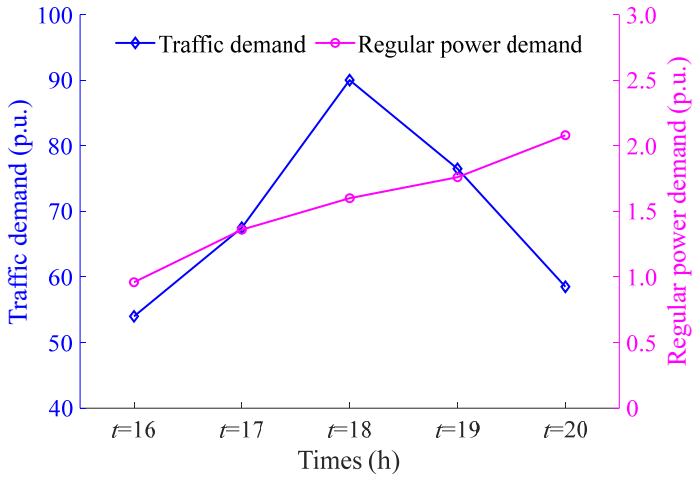

Figure 15. Initial of traffic demand and regular power demand from 16:00 to 20:00 in test system 2.

4.2.1. Effectiveness of the Proposed Distributed Coordinated Operation Model Considering IDRs in Congestion Alleviation and Cost Reduction

To further discuss and evaluate the effectiveness of the proposed distributed coordinated operation model considering IDRs in larger system, this subsection provides a detailed analysis using Cases 1, 3, and 5 as examples.

Figures 16 and 17 present the traffic flow distribution in ETN and the bus voltage levels in PDN during the afternoon commuting hours for Cases 1 and 5. In Case 1, it can be observed that the majority of traffic flows occurs at 18:00, during which the ETN experiences high traffic density, and the traffic flow on various roads is significantly higher than at other times. Simultaneously, influenced by the peak traffic demand, the peak charging load for EVs also occurs at 18:00, leading to a voltage violation at the end buses E3 and E16 in the ETN, as they fail to maintain voltage safety constraints. In contrast, Case 5 considers both the time-shifted traffic demand and regular power demand, and utilizes IDRs to regulate the departure times of traffic users and the consumption behavior of regular power users. This results in a more balanced traffic flow distribution from 16:00 to 20:00, preventing voltage violations and improving the overall operational performance of both networks.

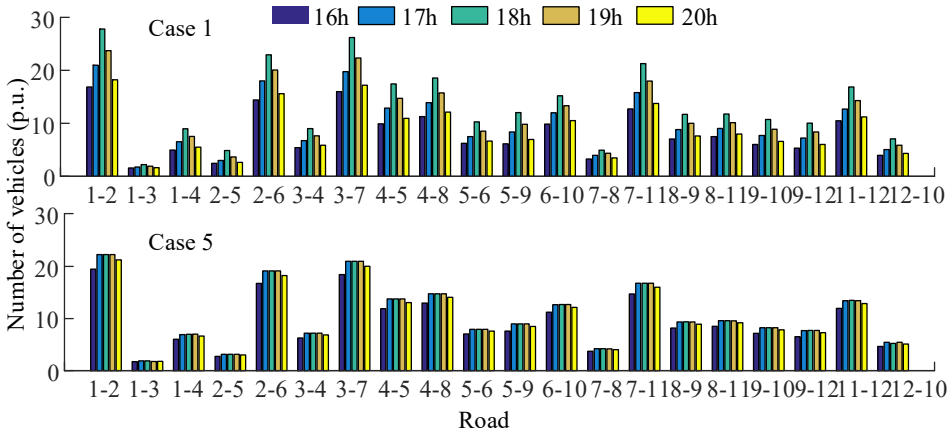

Figure 16. Traffic flow distribution of ETN from 16:00 to 20:00 in Case 1 and Case 5 in test system 2.

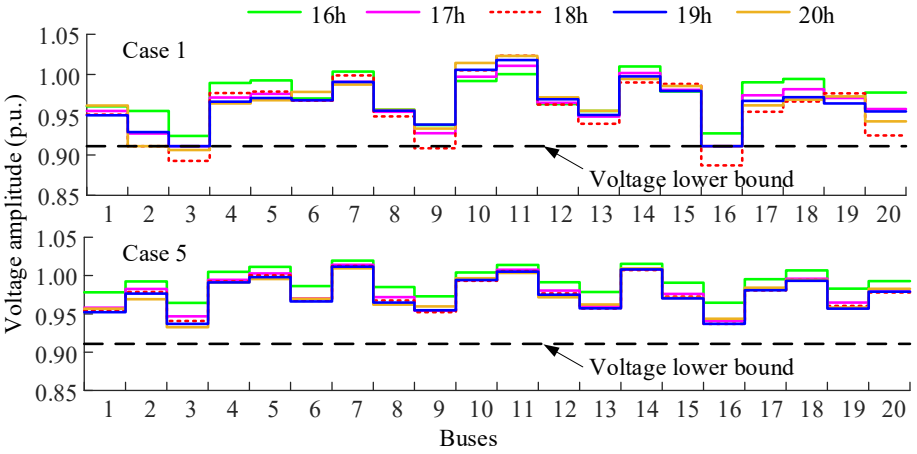

Figure 17. Node voltage level of PDN from 16:00 to 20:00 in Case 1 and Case 5 in test system 2.

Additionally, Table 7 presents the various costs of the objective function for Cases 3 and 5. It can be observed that the penalty cost for voltage violations in Case 3 is also zero, indicating that Case 3 effectively alleviates the voltage violation issues encountered in Case 1. However, compared to Case 5, Case 3 has higher total delay costs, charging costs, and total operational costs for PDN. This is because Case 3 does not consider the time-shifted traffic and regular power demand, it only achieves coordinated operation of the PDN

and ETN by adjusting the spatial distribution of traffic flow and charging loads via node marginal pricing. In contrast, Case 5 fully leverages the flexibility of both time-shiftable traffic and regular power demand, optimizing traffic and power load curves in both spatial and temporal dimensions, thus significantly reducing total delay costs for traffic users and overall PDN operating costs.

Table 7. Costs of objective function in Cases 3 and 5 in test system 2.

Cases	Total Operational Costs for ETN		Total Operational Costs for PDN		
	Total Delay Cost F_{DT} (USD)	Total Charging Cost F_{CH} (USD)	Cost of Purchasing Elec-tricity and Generation Cost F_{sub}+F_G (USD)	Penalty Cost for Load Peak-Valley Differences $F_{peak\text{-}Valley}$ (USD)	Penalty Cost for Voltage Violations (USD)
3	184,625.14	13,822.27	24,161.26	3035.19	0.00
5	175,278.99	13,746.46	23,787.11	1536.45	0.00

Therefore, the above results demonstrate that the proposed distributed coordinated operation model considering IDR is also effective in larger system.

4.2.2. Performance Analysis of the Algorithms 1 and 2

In this subsection, we examine a heavily loaded scenario (18:00 in Case 5) to assess the effectiveness of Algorithm 1, while concurrently recording the convergence of Algorithm 2 in Case 5. Additionally, we analyze the computational complexities associated with solving the MTA-TSTD and distributed coordinated operation models.

Tables 8 and 9 provide the effective travel path sets for EVs and GVs in a heavy loaded scenario (18:00 in Case 5), respectively. From Tables 8 and 9, we can observe that the proposed effective path generation model, along with solution Algorithm 1, effectively eliminates redundant routes not chosen by travelers, optimizing the effective path sets for both EVs and GVs. Moreover, travel time, travel cost, and traffic flow on these effective paths for GVs and EVs were successfully computed. It is worth noting that in cases where multiple effective paths exist between an OD pair (e.g.,T1–T11, T1–T12, T3–T10, T4–T9, T4–T10, and T4–T12 for GVs; T1–T12 for EVs), the travel costs on each path are equal, which is consistent with mixed UE state (constraints (23) and (24)). These findings strongly support the validity of the proposed ETN model and Algorithm 1.

Table 8. Effective path, travel time, travel cost, and path traffic flow for EVS (18:00 in Case 5).

Form Node	To Node	Effective Path	Travel Time (min)	Travel Cost (USD)	Traffic Flow (veh)
T1	T6	T1–T2–T6	46.45	8.41	298
T1	T10	T1–T2–T6–T10	58.94	10.90	508
T1	T11	T1–T4–T8–T11	46.22	8.55	277
T1	T12	T1–T4–T8–T11–T12	58.33	10.96	129
		T1–T2–T5–T9–T12	58.07	10.96	56
T3	T6	T3–T4–T5–T6	49.56	9.20	304
T3	T10	T3–T7–T8–T9–T10	58.49	11.05	370
T3	T11	T3–T7–T11	40.22	7.39	222
T3	T12	T3–T7–T11–T12	52.33	9.80	148
T4	T9	T4–T8–T9	42.10	7.86	92
T4	T10	T4–T8–T9–T10	52.49	9.83	185
T4	T12	T4–T8–T9–T12	51.82	9.68	277

Table 9. Effective path, travel time, travel cost, and path traffic flow for GVS (18:00 in Case 5).

Form Node	To Node	Effective Path	Travel Time (min)	Travel Cost (USD)	Traffic Flow (veh)
T1	T6	T1–T2–T6	46.45	7.74	416
T1	T10	T1–T2–T6–T10	58.94	9.82	693
T1	T11	T1–T4–T8–T11	46.22	7.70	275
		T1–T3–T7–T11	46.22	7.70	179
T1	T12	T1–T2–T5–T9–T12	58.07	9.68	258
		T1–T4–T5–T9–T12	58.07	9.68	19
T3	T6	T3–T4–T5–T6	49.56	8.26	416
T3	T10	T3–T7–T11–T12–T10	58.49	9.75	543
		T3–T7–T8–T9–T10	58.49	9.75	50
T3	T11	T3–T7–T11	40.22	6.70	340
T3	T12	T3–T7–T11–T12	52.33	8.72	247
T4	T9	T4–T8–T9	42.10	7.02	22
		T4–T5–T9	42.10	7.02	126
T4	T10	T4–T8–T9–T10	52.49	8.75	41
		T4–T5–T6–T10	52.49	8.75	71
		T4–T5–T9–T10	52.49	8.75	178
T4	T12	T4–T5–T9–T12	51.56	8.59	262
		T4–T8–T9–T12	51.56	8.59	175

Now investigate the convergence of Algorithm 2. The presented MOPF-TSPD ($P^{\mathrm{T}}_{\mathrm{Lc},s,t}-update$ subproblem (1) and MOPF-TSPD ($P^{\mathrm{E}}_{\mathrm{Lc},s,t}-update$ subproblem (2) problems are strictly convex nonlinear programming problem and second-order cone programming problem respectively, which can be efficiently solved by optimization software solvers IPOPT and Mosek, respectively. Meanwhile, due to the two problems being convex, Algorithm 2 will be able to converge to an optimal solution.

Figure 18 shows the convergence curves for the primal and dual residuals in Algorithm 2. After 15 iterations, both residuals approach zero, meeting the convergence criteria. This demonstrates that the distributed coordinated operation model for CPTES satisfies all constraints imposed by the ETN and PDN, and converges efficiently to an optimal solution.

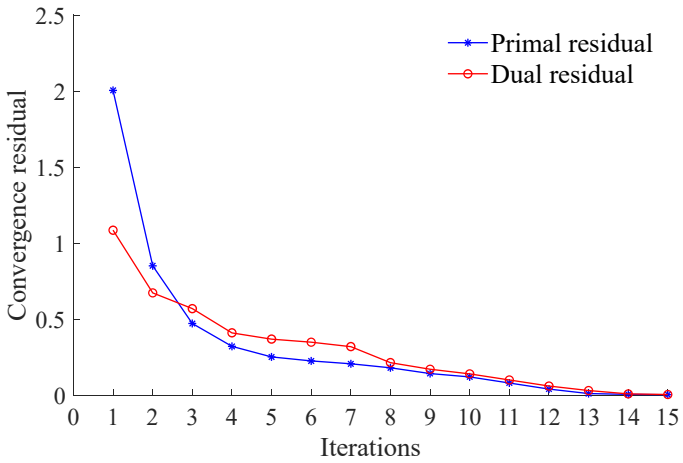

Figure 18. Convergence curves of primal and dual residuals.

Next, we analyze the computational complexity involved in solving the MTA-TSTD and distributed coordinated operation models. The computational complexity arises from three aspects: (1) Nonstandard constraints: The original MTA-TSTD includes nonstandard constraints (23) and (24), making it difficult to solve. (2) Time-shiftable traffic demands: The introduction of time-shiftable traffic demands increases model variables, adding complexity to the MTA-TSTD. 3) Effective path generation considering EV battery SOC: The

proposed model considers the EV battery SOC constraints and requires the optimization of charging energy, presenting additional challenges for path generation. These factors hinder traditional solution methods, preventing them from effectively resolving the problem. To address these challenges, we transform the MTA-TSTD into a strictly convex optimization problem with linear constraints. This transformation enables the use of efficient nonlinear solvers, such as IPOPT, which significantly enhances the model's solvability. Additionally, the effective path generation models are structured as mixed-integer quadratic programming problem. By employing solvers like CPLEX or Mosek, it can efficiently generate effective path sets while eliminating redundant paths, which further reduces computational burden. Furthermore, the distributed coordinated operation model uses decomposition techniques to break the problem into smaller, manageable subproblems, allowing for more efficient computations. Given the above approaches, Case 5 (the proposed models) can be effectively solved in about 30 min.

Figure 19 presents the computation time for each iteration of Algorithm 2 in Case 5. It can be observed that the solution time for the ETN model is significantly greater than that for the PDN in each iteration. Specifically, the average solution time for the ETN is 135 s, while the average solution time for the PDN is 0.84 s. This further demonstrates that the proposed ETN model exhibits greater computational complexity.

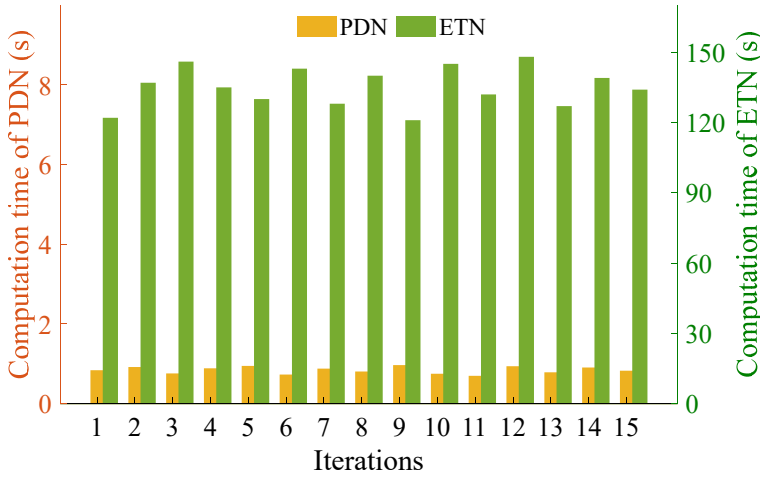

Figure 19. Computation time for each iteration of Algorithm 2 in Case 5.

5. Conclusions

In this paper, we propose a collaborative optimization framework and corresponding solution algorithms for CPTES considering IDR and EVs battery SOC. The main conclusions drawn from simulation results are as follows:

1. The MTA-TSTD effectively simulates departure times and path choices of travelers while capturing traffic flow distribution in ETN. Simultaneously, the effective path generation models with battery SOC of EVs can optimize charging energy during driving and construct the effective path sets for MTA-TSTD to reduce computational complexity.
2. The proposed distributed coordinated operation model considering IDR effectively coordinates and leverages the flexibility of time-shiftable traffic demand and regular power demand. This coordination helps reduce congestion levels and lowers total operational costs in both the ETN and PDN.
3. The developed adaptive effective path generation algorithm and ETN–PDN interaction algorithm for solving the MTA-TSTD and distributed coordinated operation model is efficient and provides reasonable solutions. The ETN–PDN interaction algorithm promotes the implementation of IDR into coordinated operation of the CPTES while ensuring data privacy between the PDN and ETN.

The effectiveness of the proposed modeling framework and corresponding solution algorithms has been demonstrated through case studies and comparisons; however, our study primarily focuses on a deterministic model and does not consider certain uncertainties, such as the random route choice of travelers due to different individual perception on travel time and charging price, and random power output of renewable distributed generators (DGs) in PDN. These factors are limitations of our current approach.

As an immediate next step, we plan to incorporate these uncertainties into the CPTES. A stochastic user equilibrium assignment model based on logit function will be adopted to describe EV routing behavior and traffic flow distribution. Additionally, we will utilize information gap decision theory (IGDT) to address the random power output of renewable DGs. Those approaches will ultimately enhance the resilience of the proposed collaborative optimization framework, thereby improving its applicability in real-world scenarios.

Author Contributions: Conceptualization, L.G. and Z.L.; methodology, L.G.; validation, L.G.; formal analysis, L.G. and C.S.; writing—original draft preparation, L.G.; writing—review and editing, L.G., C.S., D.S., Z.Z. and C.W. All authors have read and agreed to the published version of the manuscript.

Funding: This research was funded by the Doctoral Science Research Initiation Foundation of Hebei Normal University of Science and Technology (funding number: 2023YB021).

Institutional Review Board Statement: Not applicable.

Data Availability Statement: The authors confirm that the data supporting the findings of this study are available within the article.

Conflicts of Interest: The authors declare no conflicts of interest.

References

1. Poongavanam, P.; Chand, A.A.; Tai, V.B.; Gupta, Y.M.; Kuppusamy, M.; Dhanraj, J.A.; Velmurugan, K.; Rajagopal, R.; Ramachandran, T.; Prasad, K.A.; et al. Annual Thermal Management of the Photovoltaic Module to Enhance Electrical Power and Efficiency Using Heat Batteries. *Energies* **2023**, *16*, 4049. [CrossRef]
2. Barik, D.; Saeed, M.A.; Ramachandran, T. Experimental and Computational Analysis of Aluminum-Coated Dimple and Plain Tubes in Solar Water Heater System. *Energies* **2022**, *16*, 295. [CrossRef]
3. Sirisamphanwong, C.; Velmurugan, K.; Ngoenmeesri, R.; Wiengmoon, B.; Chindaruksa, S.; Ramachandran, T.; Kuppusamy, M.; Sirisamphanwong, C.; Qaisrani, M.A. Solar PV System for Thailand's International Airport: Site Configuration, Energy Production, and Glare Effect. *Int. J. Energy Res.* **2024**, *2024*, 4926504. [CrossRef]
4. International Energy Agency. Global EV Outlook 2024. 2024. Available online: https://www.iea.org/reports/global-ev-outlook-2024 (accessed on 10 May 2024).
5. Lv, S.; Sun, G.; Wei, Z.; Chen, S.; Chen, Z. Optimal Pricing and Energy Sharing of EV Charging Stations With an Augmented User Equilibrium Model. *IEEE Trans. Power Syst.* **2024**, *39*, 4336–4349. [CrossRef]
6. Yang, T.; Guo, Q.; Sheng, Y.; Sun, H. Coordination of Urban Integrated Electric Power and Traffic Network from Perspective of System Interconnection. *Autom. Electr. Power Syst.* **2020**, *44*, 1–9. [CrossRef]
7. Lv, S.; Sun, G.; Wei, Z.; Chen, S.; Zhang, H. Review of Modeling, Solution Methodology and Application for Coordinated Operation of Power and Transportation Systems. *Autom. Electr. Power Syst.* 2024; *in press*. [CrossRef]
8. Li, C.Y.; Dong, X.; Cipcigan, L.M.; Haddad, M.A.; Sun, M.Y.; Liang, J.; Ming, W.L. Economic viability of dynamic wireless charging technology for private EVs. *IEEE Trans. Transtp. Electric.* **2023**, *9*, 1845–1856. [CrossRef]
9. Liu, S.J.; Wang, D.Z.; Tian, Q.Y.; Lin, Y.H. Optimal configuration of dynamic wireless charging facilities considering electric vehicle battery capacity. *Transp. Res. E-Log.* **2024**, *181*, 103376. [CrossRef]
10. Machura, P.; Li, Q. A Critical Review on Wireless Charging for Electric Vehicles. *Renew Sustain. Energy Rev.* **2019**, *104*, 209–234. [CrossRef]
11. Lv, S.; Wei, Z.; Sun, G.; Chen, S.; Zang, H. Optimal Power and Semi-Dynamic Traffic Flow in Urban Electrified Transportation Networks. *IEEE Trans. Smart Grid* **2020**, *11*, 1854–1865. [CrossRef]
12. Lv, S.; Wei, Z.; Chen, S.; Sun, G.; Wang, D. Integrated demand response for congestion alleviation in coupled power and transportation networks. *Appl. Energy* **2021**, *283*, 116206. [CrossRef]
13. He, F.; Yin, Y.; Wang, J.; Yang, Y. Sustainability SI: Optimal Prices of Electricity at Public Charging Stations for Plug-in Electric Vehicles. *Netw. Spat. Econ.* **2016**, *16*, 131–154. [CrossRef]
14. Wei, W.; Wu, L.; Wang, J.; Mei, S. Network Equilibrium of Coupled Transportation and Power Distribution Systems. *IEEE Trans. Smart Grid* **2018**, *9*, 6764–6779. [CrossRef]
15. Geng, L.; Lu, Z.; He, L.; Zhang, J.; Li, X.; Guo, X. Smart charging management system for electric vehicles in coupled transportation and power distribution systems. *Energy* **2019**, *189*, 116275. [CrossRef]

16. Qian, T.; Shao, C.; Li, X.; Wang, X.; Shahidehpour, M. Enhanced Coordinated Operations of Electric Power and Transportation Networks via EV Charging Services. *IEEE Trans. Smart Grid* **2020**, *11*, 3019–3030. [CrossRef]
17. Xie, S.; Wu, Q.; Hatziargyriou, N.D.; Zhang, M.; Zhang, Y.; Xu, Y. Collaborative Pricing in a Power-Transportation Coupled Network: A Variational Inequality Approach. *IEEE Trans. Power Syst.* **2023**, *38*, 783–795. [CrossRef]
18. Shao, C.; Li, K.; Qian, T.; Shahidehpour, M.; Wang, X. Generalized User Equilibrium for Coordination of Coupled Power-Transportation Network. *IEEE Trans. Smart Grid* **2023**, *14*, 2140–2151. [CrossRef]
19. Shao, C.; Li, K.; Li, X.; Hu, Z.; Shahidehpour, M.; Wang, X. A Decentralized Bi-Level Decomposition Method for Optimal Operation of Electric Vehicles in Coupled Urban Transportation and Power Distribution Systems. *IEEE Trans. Transp. Electrif.* **2024**, *10*, 2235–2246. [CrossRef]
20. Hu, L.; Wei, W.; Shen, Z. Impact of Time-shiftable Traffic Demands on Coupled Transportation and Power Distribution Systems. In Proceedings of the IEEE Innovative Smart Grid Technologies-Asia (ISGT Asia), Chengdu, China, 21–24 May 2019.
21. Jiang, H.; Zhang, Y.; Chen, Y.; Zhao, C.; Tan, J. Power-traffic coordinated operation for bi-peak shaving and bi-ramp smoothing—A hierarchical data-driven approach. *Appl. Energy* **2018**, *229*, 756–766. [CrossRef]
22. Zhou, Z.; Zhang, X.; Guo, Q.; Sun, H. Analyzing power and dynamic traffic flows in coupled power and transportation networks. *Renew. Sustain. Energy Rev.* **2021**, *135*, 3130384. [CrossRef]
23. Xie, S.; Xu, Y.; Zheng, X. On Dynamic Network Equilibrium of a Coupled Power and Transportation Network. *IEEE Trans. Smart Grid* **2022**, *13*, 1398–1411. [CrossRef]
24. He, F.; Yin, Y.; Zhou, J. Integrated pricing of roads and electricity enabled by wireless power transfer. *Transp. Res. Part C Emerg. Technol.* **2013**, *34*, 1–15. [CrossRef]
25. Manshadi, S.D.; Khodayar, M.E.; Abdelghany, K.; Uster, H. Wireless Charging of Electric Vehicles in Electricity and Transportation Networks. *IEEE Trans. Smart Grid* **2018**, *9*, 4503–4512. [CrossRef]
26. Wei, W.; Mei, S.; Wu, L.; Shahidehpour, M.; Fang, Y. Optimal Traffic-Power Flow in Urban Electrified Transportation Networks. *IEEE Trans. Smart Grid* **2017**, *8*, 84–95. [CrossRef]
27. Liu, J.C.; Zhang, H.Y.; Liu, A.Y.; Cao, S.Q. Operation Mechanism and Co-optimization for Electrified Transportation-Distribution Networks with Dynamic Wireless Charging. *Autom. Electr. Power Syst.* **2022**, *46*, 107–118. [CrossRef]
28. Wei, W.; Mei, S.; Wu, L.; Wang, J.; Fang, Y. Robust Operation of Distribution Networks Coupled With Urban Transportation Infrastructures. *IEEE Trans. Power Syst.* **2017**, *32*, 2118–2130. [CrossRef]
29. Geng, L.; Lu, Z.; Guo, X.; Zhang, J.; Li, X.; He, L. Coordinated operation of coupled transportation and power distribution systems considering stochastic routing behaviour of electric vehicles and prediction error of travel demand. *IET Gener. Transm. Distrib.* **2021**, *15*, 2112–2126. [CrossRef]
30. Sheffy, Y. *Urban Transportation Networks: Equilibrium Analysis with Mathematical Programming Methods*; Traffic Engineering Control; Prentice Hall: Hoboken, NJ, USA, 1985.
31. Fisk, C. Some developments in equilibrium traffic assignment. *Transport. Res. Part B* **1980**, *14*, 243–255. [CrossRef]
32. Mohsenian-Rad, A.H.; Wong, V.W.S.; Jatskevich, J.; Schober, R.; Leon-Garcia, A. Autonomous demand-side management based on game-theoretic energy consumption scheduling for the future smart grid. *IEEE Trans. Smart Grid* **2010**, *1*, 320–331. [CrossRef]
33. Kirschen, D.S. Demand-side view of electricity markets. *IEEE Trans. Power Syst.* **2003**, *18*, 520–527. [CrossRef]
34. Farivar, M.; Low, S. Branch flow model: Relaxations and convexification. *IEEE Trans. Power Syst.* **2013**, *28*, 2554–2572. [CrossRef]
35. Huang, S.J.; Wu, Q.W.; Wang, J.H.; Zhao, H.R. A sufficient condition on convex relaxation of AC optimal power flow in distribution networks. *IEEE Trans. Power Syst.* **2017**, *32*, 1359–1368. [CrossRef]
36. Boyd, S.; Parikh, N.; Chu, E.; Peleato, B.; Eckstein, J. Distributed optimization and statistical learning via the alternating direction method of multipliers. *Found Trends Mach Learn* **2011**, *3*, 1–122. [CrossRef]